An interconnected palaeo-subglacial lake system in the central Barents Sea

Mariana Esteves, Denise C. Rüther, Monica C. M. Winsborrow, Stephen J. Livingstone, Calvin Shackleton, Karin Andreassen, Wei-Li Hong, Jochen Knies

---

Please note that this manuscript was previously submitted to Boreas in 2018 and underwent the peer-review process. The reviewers' comments were addressed and the appropriate changes were made in the text and figures, prior to the manuscript submission being withdrawn from the journal by the main author as additional time was required to complete the sulphate and chloride analyses.

This EarthArXiv preprint manuscript (version 1) is therefore non-peer reviewed, although it includes the changes suggested during the last peer-review process.

Subsequent versions of this preprint manuscript may thus contain slightly different content once this manuscript is resubmitted.

An interconnected palaeo-subglacial lake system in the central Barents Sea

Mariana Esteves*, Denise C. Rüther, Monica C. M. Winsborrow, Stephen J. Livingstone, Calvin Shackleton, Karin Andreassen, Wei-Li Hong, Jochen Knies

Drainage of meltwater beneath an ice sheet influences ice-flow dynamics. To better predict ice sheet behaviour, it is crucial to understand subglacial hydrological processes. Subglacial lakes are important components of the subglacial hydrological system, with many observed and predicted at the beds of contemporary and palaeo-ice sheets. The technical and logistical challenges of studying subglacial lakes in Antarctica and Greenland have motivated recent efforts to reliably identify often more accessible palaeo-subglacial lakes, which serve as valuable geological analogues. In this paper, we present a suite of sediment records from an interconnected basin and channel system in the central Barents Sea, inferred to represent a palaeo-subglacial lake system based on glacial geomorphological mapping. We observe clear lithological differences between cores extracted within and outside the basins. Cores from within the basins are characterised by winnowed till or rain-out till overlain by high- to low-energy sediment deposits, consistent with irregular flushing of meltwater followed by ice proximal conditions. We identify varying degrees of hydrological activity between basins, with those well-connected by meltwater channels characterised by winnowed till, while the more marginal basins are associated with thick rain-out till deposits. This work provides the first geomorphological and sedimentological record of a dynamic and active palaeo-subglacial lake system in the central Barents Sea.

Keywords

Barents Sea Ice Sheet; Late Quaternary; Palaeo-subglacial lakes; Subglacial hydrology; Marine-based ice sheet; Sedimentology.

*Mariana Esteves (*Corresponding author: mariana.esteves@uit.no), Monica C. M. Winsborrow, Karin Andreassen, Calvin Shackleton, Jochen Knies, Centre for Arctic Gas Hydrate, Environment and Climate (CAGE), Department of Geosciences, UiT the Arctic University of Norway, 9037 Tromsø, Norway; Denise C. Rüther, Western Norway University of Applied Science (HVL), Sogndal, Norway; Stephen J. Livingstone, Department of Geography, Sheffield University, Winter Street, Sheffield, S10 2TN, UK; Wei-Li Hong, Jochen Knies, Geological Survey of Norway, NO-7491, Trondheim, Norway. Calvin Shackleton, Norwegian Polar Institute, Fram Senteret, Tromsø, Norway.*

1. Introduction

The presence and distribution of meltwater at the ice-bed interface has a primary control on the dynamics and behaviour of the overlying ice sheet (Bell, 2008), through its influence on basal frictional resistance and subglacial sediment strength (e.g. Alley et al., 1986; Engelhardt and Kamb, 1997; Tulaczyk et al., 2000). In addition, increased subglacial water pressures can promote ice velocity accelerations (Zwally et al., 2002; Vaughan et al., 2013), and channelised drainage configurations associated with lower water pressures, can promote ice flow decelerations (e.g. Röthlisberger, 1972; Alley et al., 1994; Bougamont et al., 2003; Bartholomew et al., 2010; Andrews et al., 2014). The volume of subglacial meltwater and its distribution beneath an ice sheet can undergo rapid changes both spatially and temporally, triggering significant changes in ice sheet dynamics.

Subglacial lakes are important components of the hydrological network and have the potential to store and drain large volumes of freshwater on decadal to centennial timescales (Wingham et al., 2006; Fricker and Scambos, 2009; Palmer et al., 2013, Siegert et al., 2014). Lake drainage events have been directly linked to transient downstream ice velocity accelerations during the period of lake discharge (Stearns et al., 2008). Since the first subglacial lake was identified in Antarctica from airborne radio-echo sounding data (Robin et al. 1970; Oswald and Robin, 1973), we now understand these to be relatively common features, forming part of a complex subglacial hydrological network of over 380 subglacial lakes and extensive interconnected channelised systems beneath the Antarctic Ice Sheet (Kapitsa et al., 1996; Siegert, 2005; Wingham et al., 2006; Fricker et al., 2007; Smith, 2009; Wright and Siegert, 2012). Several subglacial lakes have been identified beneath the Greenland Ice Sheet (e.g. Palmer et al., 2013), and subglacial hydraulic potential modelling (Livingstone et al., 2013a,b; Shackleton et al., 2018) indicates the potential for thousands more subglacial lakes to exist/have existed beneath contemporary- and palaeo-ice sheets.

Given the influence of meltwater on ice sheet behaviour, improving our knowledge of how subglacial hydrological networks are organised and behave over long and short timescales represents a key research priority. However, accessing contemporary meltwater channels and subglacial basins, as well as the sediments therein, remain a logistical challenge, and while there have been several attempts to core contemporary subglacial lakes, such as Lake Whillans (e.g. Hodson et al., 2016), our understanding of these environments has largely relied on theoretical or indirect geophysical data (e.g. Livingstone et al., 2012). For this reason, geomorphic and sedimentary archives from palaeo-settings are important for providing wider spatial and temporal perspectives on subglacial hydrology.

Palaeo-subglacial lakes are difficult to identify in the geological record due to their uncertain geomorphological and sedimentological expressions, as well as difficulties in distinguishing between proglacial and subglacial sediments (e.g. Livingstone et al., 2012, 2015). Bentley et al. (2011) and Livingstone et al. (2012) also present a comprehensive diagnostic criteria, highlighting many of the dominant processes occurring within a subglacial lake. This includes reorganisation and deposition of sediments from processes such as melt-out from basal debris-rich ice, subaqueous debris/turbidity-flows (i.e. underflows), suspension settling from overflows, ice-grounding events, flushing events, and periodic infilling/drainage events.

Recent work combining geophysical, geomorphological and sedimentological data outlines a distinctive landsystem suggested to be indicative of an active subglacial lake environment. This consists of flat spots or basins, interpreted as former subglacial lakes connected by subglacial meltwater channels that were incised during lake drainage (e.g. Livingstone et al., 2016; Simkins et al., 2017; Kuhn et al., 2017). Furthermore, low-chloride pore water concentrations of sediment in a basin in Pine Island Bay, Antarctica have been used to indicate deposition in a freshwater subglacial lake setting (Kuhn et al., 2017). This inference is supported by a distinctive sediment facies, including the presence of structureless silty clay, which indicates deposition in an enclosed, low-energy lacustrine environment (Kuhn et al., 2017).

In this paper, we examine an area in the central Barents Sea which contains a complex system of basins interconnected by small channels incised into the seafloor (figs. 1-3). There is extensive evidence for subglacial meltwater activity in this area (Bjarnadóttir et al., 2014, 2017; Esteves et al., 2017; Newton and Huuse, 2017), and previous work has postulated that palaeo-subglacial lakes occupied these interlinked basins (Esteves et al., 2017). In this paper, we combine results from five sediment cores with previously published and new glacial geomorphological mapping of an interconnected basin and channel system on Thor Iversenbanken, central Barents Sea (figs. 2 and 3). We strengthen the argument that area hosted palaeo-subglacial lakes during the last deglaciation based on the glacial geomorphology and clear differences in the sedimentological record between cores collected from within the basins, and on the adjacent bank. This work is the first sedimentological study of palaeo-subglacial lakes in the Barents Sea.

2. Background

2.1. Geological/oceanographic setting

The Barents Sea is a large epi-continental sea, characterised by shallow banks (100-200 mbsl) and deeper troughs (300-500 mbsl; fig. 1). The Quaternary sediments within the Barents Sea overlie Mesozoic and early Cenozoic bedrock and are generally thin (<10-15 m) due to extensive erosion during successive glaciations (Elverhøi et al., 1993). The geology subcropping the unlithified sediments within and around the study area on the northwestern flanks of Thor Iversenbanken is predominantly Early Cretaceous with some smaller areas of mid- to late-Cretaceous, late-Jurassic to early-Cretaceous, and early- to mid-Triassic bedrocks (Sigmond, 1992). South of the area, are large early Permian salt deposits and Palaeocene rocks (Sigmond, 1992).

The Arctic Polar Front crosses the Barents Sea between 74°-75° and is the intersection between warm, saline North Atlantic waters and the cooler, low-salinity Arctic waters (Loeng, 1991; Pfirman et al., 2013). These currents are funnelled by bathymetric features and in the central Barents Sea, the Arctic Polar Front coincides with the 200 m contour line. The Barents Sea experiences high bottom water currents, with maximum velocities reaching 25-30 cm/s at water depths of 270 m (Loeng, 1983). In particular, high velocities occur along the Polar Front, which passes over the study area. This promotes the winnowing and erosion of shallow banks due to strong currents and the influence of tidal and storm activity, as observed on Spitsbergenbanken (Elverhøi et al., 1989). For this reason, preservation and sedimentation of Holocene material is limited, with low accumulation rates of 2-5 cm/ka (Elverhøi et al., 1989; Vorren et al., 1989).

2.2. Glaciological setting

Throughout the Cenozoic, the Barents Sea experienced multiple glaciations (Elverhøi and Solheim, 1983; Vorren et al., 1988; Vorren and Laberg, 1997), the most recent of which peaked during the Late Weichselian (~18-21 cal. ka BP) when the marine-based Barents Sea Ice Sheet (BSIS) extended to the western and northern continental shelf breaks, coalescing with the Fennoscandian Ice Sheet to the south (Landvik et al., 1998; Svendsen et al., 2004; Hughes et al., 2016; Patton et al. 2015, 2016). The BSIS is a good palaeo-analogue for the West Antarctic

Ice Sheet, since they are both marine based ice sheets, overlying sedimentary bedrock and were of similar sizes during Last Glacial Maximum (LGM; Andreassen and Winsborrow, 2009).

The BSIS had several ice streams that occupied the cross-shelf troughs during the LGM and subsequent deglaciation, the largest of which was the Bjørnøyrenna Ice Stream, with an estimated maximum catchment area in excess of 350,000 km^2 (Vorren and Laberg, 1997; Andreassen et al., 2004; Winsborrow et al., 2010a; Andreassen et al., 2014). This catchment encompassed several major ice-tributaries, among them ice flowing from Storbankrenna and Sentralbankrenna (Bjarnadóttir et al., 2014, Esteves et al., 2017; Newton and Huuse et al., 2017; Patton et al., 2017), the latter of which was adjacent to our study area (fig.1).

Both empirical and modelling studies indicate rapid periods of ice retreat with intermittent margin still-stands, as the BSIS deglaciated from its maximum extent at the continental shelf break (e.g. Andreassen et al., 2008, 2014; Winsborrow et al., 2010a; Bjarnadóttir et al., 2014, Patton et al., 2017). The Bjørnøyrenna Ice Stream had retreated from the shelf edge in the southwestern Barents Sea by 17.1 cal. ka BP (Rüther et al., 2011) and deglaciation in the central Barents Sea occurred between 16-14 cal. ka BP (Salvigsen, 1981; Winsborrow et al., 2010a; Hughes et al., 2016). In the central Barents Sea, the mouth of Sentralbankrenna, (~70 km west from our study site) is suggested to have been fully deglaciated by 13.9 cal. ka BP (Rise et al., 2016) and Sentraldjupet, in the southeastern Barents Sea, by 15.1 cal. ka BP (Polyak et al., 1995). However, despite a good understanding of how the ice streams retreated, chronological control on deglaciation in the central Barents Sea remains poor, largely due to the scarcity of available dateable material.

3. Datasets and methods

The study area is located on the northwestern flank of Thor Iversenbanken, central Barents Sea, at a water depth ranging from 190-340 mbsl (figs. 1 and 2). Here, several basin-like depressions were observed and suggested through geomorphological studies to have hosted palaeo-subglacial lakes (Esteves et al., 2017). Five sediment gravity cores were collected during a CAGE (Centre for Arctic Gas Hydrate, Environment and Climate) research cruise on-board the R/V Helmer Hanssen in 2015 and analysed in order to get a better understanding and overview of the different depositional environments and in particular the subglacial hydrological setting, within this study area. Cores 1222, 1225, and 1230 were collected from the deepest parts of the lower, middle, and upper basins respectively, whereas core 1228 was taken from the margin of the middle basin, and core 1221 from the lee-side of the adjacent bank area (fig. 2; table 1). Core extraction sites were decided based on chirp profiles collected prior to coring, as well as the glacial geomorphological mapping of the area (fig. 2; Esteves et al., 2017).

The gravity cores were collected using a 3 m long barrel, with an inner diameter of 10.2 cm. Once on-board, cores were split, described and measured for the undrained shear strength using the fall cone test (Hansbo, 1957). A total of 204 samples were taken at 10 cm intervals plus intervals of interest for water content measurements, grain-size analysis and for picking of foraminifera. In addition to this, a further 64 samples for measurements of chloride and sulphate concentrations were taken at every 10 cm interval as soon as the cores were split and stored at -20°c. In early 2017 pore water was extracted through centrifuging (4000 rpm for 20 minutes) and filtering with 0.2 µm inline syringes before being stored under 4°c. Concentrations of sulphate and chloride were analysed in 2018 using a Dionex ICS-1100 Ion Chromatograph with a Dionex AS-DV autosampler and a Dionex IonPac AS23 column (eluent: 4.5 mM Na2CO3/0.8 mM NaHCO3, flow: 1ml/min) at the Geological Survey of Norway. The relative standard deviations from repeated measurements of different laboratory standards are better than 0.5% for concentrations above 0.1 mM and better than 1.8% for concentrations above 0.02 mM. We assume that while some minor alteration as a result of evaporation during core storage may have occurred that the results still preserve the original signals.

Sufficient material for radiocarbon dating was found at two depths (30-31 cm in core 1221 and 10-11 cm in core 1230), which was performed at Poznań Radiocarbon laboratory, Poland (Table 2). The age calibration for our own as well as cited radiocarbon dates was run using Calib 7.1. Software (Stuiver and Reimer, 2017) with the application of the Marine13 calibration curve (Reimer et al., 2013) and a regional correction of ΔR=71±21 with respect to the global mean marine reservoir age (Mangerud et al., 2006). The samples presented here contained very low quantities of carbon (0.13 mgC for the sample in core 1221, and 0.2 mgC for the sample in core 1230) and thus, should be considered carefully.

Grain size analyses on standard sedimentological size fractions (Friedman and Sanders, 1978) were performed on 102 samples using a Beckman Coulter LS 13 320 Particle Size Analyzer. Clasts larger than 2 mm were counted from x-radiographs at 2 cm intervals using the Grobe (1987) method. The core halves were subsequently x-rayed with a Geotek MSCL-XCT x-ray imaging system. High-resolution photographs were taken with an Avaatech X-ray Fluorescence (XRF) core scanner.

Glacial geomorphological mapping was undertaken by Esteves et al. (2017) with some further carried out using high-resolution (5 m) multibeam bathymetric data, provided by the MAREANO Programme (www.mareano.no). Detailed mapping and visualisation of glacial landforms was undertaken using Esri ArcMap v10.1 and QPS Fledermaus. Chirp data was collected during the 2015 CAGE research cruise, using X-STAR Full Spectrum Sonar chirp subbottom profiler, which is a hull mounted chirp system, operating at 4 kHz with a shot rate of 1 second. Chirp data have been analysed and visualised using the Kingdom software 8.8.

4. Results

4.1. Glacial geomorphology

Located on the northwestern flank of Thor Iversenbanken (fig. 1), the study area lies between three large arcuate recessional moraines on Thor Iversenbanken (fig.2) and a deeper trough, Sentralbankrenna that displays large grounding-zone wedges and mega-scale glacial lineations to the west (fig. 3). This area is located close to a postulated shear margin between slower moving bank ice on Thor Iversenbanken, and a fast-flowing ice stream in Sentralbankrenna (Bjarnadóttir et al., 2014, 2017; Esteves et al., 2017; Newton and Huuse, 2017). Several meltwater channels and tunnel valley incised into the seafloor breach ice marginal deposits in the area, which comprise of recessional moraines (figs. 2 and 3), indicating that these channels were active during the later-phases of local deglaciation.

The tunnel valley has an undulating long-profile, which shallows towards its mouth, and is ~32 m deep, ~50 km long, and ~310 m wide (fig. 3A; Bjarnadóttir et al., 2017; Esteves et al., 2017; Newton and Huuse, 2017). All of the meltwater channels are orientated SE-NW, towards the trough, and terminate west of the slope break, where a small channel runs southwards, parallel to the trough. Previous studies have proposed the tunnel valley formed subglacially and gradually over time, whilst experiencing occasional outburst floods possibly originating from palaeo-subglacial lake drainage events (Bjarnadóttir et al., 2017; Esteves et al., 2017; Newton and Huuse, 2017). A proglacial origin for the channels is excluded given the marine-terminating ice margin and their undulating long profile.

Upstream of the tunnel valley are three basin-like depressions that have numerous channels leading into and out of them, forming an interconnected hydrological network (figs. 2 and 3; Esteves et al., 2017). These basins are separated by bathymetric highs (10-15 m) and are <20 m deep, ~2-4 km long, ~1-1.5 km wide, and occur at water depths between 300-310 mbsl. These bathymetric highs may have provided a pinning point for the ice margin during its overall retreat over the area. The minimum water volume capacities for the upper, middle, and lower basins are estimated to be 0.0002 km^3, 0.0019 km^3 and 0.0013 km^3, respectively, with the combined water volume capacities approximately 0.0034 km^3 (fig. 3C). These water volumes capacities are similar to those calculated for the palaeo-subglacial lakes observed in the Ross Sea, Antarctica (Simkins et al., 2017). However, while post-glacial sedimentation is relatively low in the Barents Sea, uncertainties relating to the exact water volume capacities of the basins are likely to occur as they might have experienced some open-marine Holocene sediment infill.

The chirp penetration in the area is generally low with only shallow sedimentary units (~2-10 m) visible within the basins (fig. 2C and D). The thickest unit (~10 m) in the profile crossing the middle basin (fig. 2C) appears to have at least two subsurface reflections. However, due to the low penetration of the subsurface chirp dataset, the exact thicknesses, spatial distribution, and internal architecture of the sediments within the basins, channels and esker remain difficult to ascertain (fig. 2C and D). Furthermore, the chirp data does not penetrate into the bathymetric highs between the basins, providing uncertainties if these are bedrock or glacigenic material formed during sediment deposition during late-stage ice margin retreat or whether they were formed subglacially during an earlier stage of deglaciation or LGM.

These basins are interlinked by meltwater channels incised into the seafloor and eventually join downstream forming the tunnel valley that leads into Sentralbankrenna. The lower and middle basins have considerably more channels leading into and out of the basins, unlike the upper basin, which has one small channel crossing the basin at its northwestern corner (figs. 2A and 3). Only three areas with eskers are observed (figs. 2A and 3B). These eskers are located around the lower basin and are orientated in a SE-NW direction parallel to the channels. They are between 550-1000 m in length, 40-45 m wide, and 2-4 m height (figs. 2A and 3B).

4.2. Lithostratigraphy

Using a combination of observed facies and physical properties, we defined three primary lithological units (fig. 4A-E). Each of these units represents a major glacial environment or process. The results and interpretations of these units are presented in order of oldest (unit 3) to youngest (unit 1). The distinctions based on lithological characteristics, shear strength, water content, and lower unit boundaries are detailed in table 3, with further descriptions of the units below.

4.2.1. Unit 3 – Dark grey consolidated diamict

Results

Unit 3 is observed in all of the sediment cores and consists of consolidated, very dark-to-dark grey, predominantly structureless diamict (fig. 4). Based on clast and water content as well as variations in lithostratigraphy, this unit is divided into three subunits: subunit 3a, present in core 1221; subunit 3b, present in cores 1222 and 1225; and subunit 3c present in cores 1228 and 1230 (fig. 4). Subunit 3a has a homogeneous silty matrix with low sand content and relatively low water content (on average ~12%), and shear strengths ranging between 6.8-21 kPa. It is crudely stratified over a 5 cm interval occurring at a depth around 45-50 cm (figs. 4A and 5A). Subunit 3b is composed of sandy-mud and sandy-silt and has a high clast count and large clasts (figs. 4B and C, and 5B). The water content is very low (on average ~5%), shear strengths range from 6-37.5 kPa and the sand content in the matrix increases up-unit (fig. 4B and C). Subunit 3c is characterised by relatively low clast content with patches of sandy-mud and sandy-silt, and has a low water content (on average ~12 %), with shear strengths ranging from 6.8-27.5 kPa (figs. 4D and E, and 5C). Chloride and sulphate concentrations remain within the normal ranges for marine sediments within all of the cores.

Interpretation

Based on its predominantly massive character, heterogeneity of grain sizes, and increased shear strength we interpret unit 3 to represent subglacial diamict (e.g. Powell and Alley, 1997; Ó Cofaigh et al., 2007). The structureless part of subunit 3a is characteristic of a subglacial traction till (e.g. Evans, 2006), and the crude stratification present within a small section of this subunit may have occurred due to ice-bed decoupling (Piotrowski et al., 2006) or the occurrence of local brittle deformation possibly due to a reactivated cold glacial bed (Hooke and Iverson, 1995; Piotrowski et al., 2006). An alternative interpretation for subunit 3a, is that it represents a mass flow deposit formed at the ice margin of a subglacial lake cavity through the deformation of till and rain-out of sediment near the influx point, similarly to that observed by McCabe and Ó Cofaigh (1994). However, we favour the former explanation. The high clast content in subunit 3b, together with its low water content, is consistent with a winnowed till origin in an environment with high bottom currents promoting the removal of finer sediment. This interpretation is also consistent with the up-unit increase of sand content in the matrix. Based on its relatively homogeneous, massive sandy-mud to sandy-silt matrix, with several patches of sandy-mud and interspersed clasts, subunit 3c is interpreted as a rain-out till, a diamicton deposited by a combination of rain-out, current re-working and flow remobilization. (e.g. Evans and Pudsey, 2002).

4.2.2. Unit 2 – dark olive-brown to dark grey partly laminated sequences

Results

Unit 2 is observed in all of the cores and consists of partly laminated dark grey to dark olive-brown sandy-mud/silt to silt (figs. 4 A-E). The shear strength is relatively low (on average ranging between 4.6-7.75 kPa; table 3), with locally higher values correlating with increased sand content. Based on differences in lithology and structures, this unit is divided into three subunits (table 3). Subunit 2a is present in cores 1221 and 1222 and consists of a laminated sandy-silt interval that transitions up-core into a homogeneous silt matrix with rare dropstones. It has a low shear strength and high water content (7.75 kPa and 20.64 % respectively). Sufficient bulk foraminifera for radiocarbon dating were collected from the silt laminations in core 1221, returning a calibrated age estimate of 39.7 cal. ka BP (table 2; fig. 4A).

Subunits 2b and 2c are present in all but core 1221 and consist of up-core fining sequences from sandy-silt to silt, and in some cores from sandy-mud to sandy-silt. The subunits are generally coarser in cores 1228 and 1230 compared to cores 1222 and 1225 (fig. 4). Subunits 2b and 2c have clear erosional bases and contain plane parallel and ripple laminations. The water content in subunits 2b and 2c is moderately high (on average 21.58 % and 16.52 % respectively). Subunit 2c shows no signs of biological activity, whilst in the upper parts of subunit 2b shell fragments, burrows and hydrotrollites are visible (fig. 4).

Interpretation

Subunit 2a can be distinguished based on its relatively low shear strength, occurrence of laminations and layering, as well as the presence of occasional dropstones, which are all consistent with a glaciomarine origin (e.g. Powell and Domack, 1995; fig. 5D). However, the date from the lower laminated interval returned an age of 39.7 cal. ka BP in core 1221. If correct, this would suggest a pre-LGM age for this unit. Exceptionally high shear strength immediately above the laminations in subunit 2a may represent grounding of ice during the LGM and subsequent homogenous silt would then correspond to deglaciation material deposited post-LGM. However, we find this scenario unlikely given the poor preservation potential of previous deglacial sediments. We instead suggest that all of subunit 2a was deposited during final deglaciation encompassing reworked biological material thus yielding a non-*in situ* age.

Subunits 2b and 2c share many of characteristics typical of glaciomarine sediments (e.g. Powell and Domack, 1995), however, the observed laminations and up-core fining sequences indicate two episodes of rapid transition from high to low energy sediment environments (fig. 5E and F). The sediment facies could either represent variations in bottom current strength or incomplete Bouma sequences Ta to Te (formed by turbidite deposits; cf. Bouma, 1962; fig. 5E and F|). The Bouma units are as follows: Ta) massive to normally graded structures; Tb) planar parallel laminations; Tc) Ripples and wavy lamination; Td) upper parallel lamination; Te) homogeneous to laminated (Bouma, 1962). These characteristics can be observed within units 2c and 2b with varying degrees of completeness may suggest that the depositional setting was confined, possibly in a cavity under perennial sea-ice, an ice shelf or in a subglacial lake. Alternatively, these sedimentary units may be indicative of two high- to low-energy deposition sequences within a subglacial lake close to the ice margin and later ice-proximal to the ice margin. We favour this interpretation of the units based on the combination of sedimentological and geochemical results, which indicate that there was no freshening of the sediment pore water and grain size distributions indicate up-core fining sequences with some coarser laminations within. Small quantities of shell fragments, burrows and hydrotrollites towards the top of subunit 2b indicate an important environmental transition into glaciomarine (subunit 2a) and later open marine conditions (unit 1; fig. 4).

4.2.3. Unit 1 – Relatively homogeneous sandy-mud

Results

Unit 1 is the shallowest unit in all of the cores and gradually transitions from a dark grey to olive grey/greenish-brown, sandy-mud to sandy-silt sediment (figs. 4 A-E). Unit 1 has low shear strength (on average 5.17 kPa), relatively high water content (on average 20.30%) and low clast content (fig. 4). This unit shows abundant signs of biological activity such as shell fragments, burrows, as well as hydrotrollite layers and nodules (figs. 4 B-E, and 5 G). It is well preserved in the cores from inside the basins; the thickest units are in the deepest cores (48 cm and 80 cm in cores 1222 and 1225 respectively) and the shallower cores reveal thinner units (10 cm, 27 cm and 17 cm in cores 1221, 1228 and 1230 respectively; figs. 4 A-E). Sufficient bulk foraminifera were obtained from unit 1 in core 1230, providing a calibrated radiocarbon age estimate of 1165 cal. years BP (table 2).

Interpretation

Unit 1 represents open marine Holocene sedimentation. This is supported by a radiocarbon age of 1165 cal years BP in core 1230. Water depth plays an important role in Holocene deposition within the Barents Sea with little to no deposition on bank areas shallower than 300 m and deposition of biogenic and winnowed material in areas deeper than 300 m (Elverhøi et al. 1989). This trend can be recognised in our cores, with the shallowest core location (bank area – core 1221) having the thinnest unit and the deeper cores (lower and middle basins – cores 1222 and 1225) showing the thickest and better preserved units (fig. 4).

5. Discussion

Using a combination of glacial geomorphological and sedimentological datasets, we propose that this area hosted palaeo-subglacial lakes and that differences in the hydrological regime and depositional environments can be observed. The following sections integrate both datasets to discuss indications for palaeo-subglacial lakes and the style of hydrological regimes within these, prior to elaborating on a possible model of palaeo-subglacial formation on Thor Iversenbanken.

5.1. Indications for the presence of palaeo-subglacial lakes on Thor Iversenbanken

The glacial geomorphology of Thor Iversenbanken reveals three main basins connected by meltwater channels incised into the seafloor, which converge downstream of the basins into a large dendritic channel system and tunnel valley (figs. 2 and 3; Esteves et al., 2017). Based on the morphology and size of the basins, in combination with the extensive channel system, we suggest that shallow, transient subglacial lakes may have been present. Similarly to palaeo-subglacial lakes identified in Canada (Livingstone et al., 2016) and on the Antarctic continental shelf (Kuhn et al., 2017; Simkins et al., 2017), these palaeo-subglacial lakes may have undergone periodic drainage through a channelised system. Hydraulic potential modelling of the subglacial drainage routing in the Barents Sea further supports the presence of extensive subglacial meltwater in this region (Shackleton et al., 2018; fig. 6A).

Core 1221, collected in the bank area (fig. 2), displays a deglacial sedimentary record (e.g. Elverhøi et al., 1989; Vorren et al., 1989), consisting of a transition from subglacial traction till (subunit 3a; fig. 4A), into a classic glaciomarine deposit (subunit 2a), to open-marine deposits typical for shallow bank areas (unit 1; fig. 4A). In contrast, cores collected from within and at the margin of the basins (cores 1222, 1225, 1228, 1230) contained subunits less characteristic of the typical deglacial sediment sequences.

Common to all cores from the basins is the presence of two high- to low-energy depositional sequences (subunits 2c and 2b; figs. 4B-E and 5E and F). The coarser nature of sequences in the upper basin (core 1230) may be due to its position more proximal to the grounding line, and thus influx point, of the subglacial lake cavity (figs. 2 and 3). We suggest that these subunits formed by turbidity flows originating from sediment-laden subglacial meltwater inflowing from subglacial channel(s) at the subglacial lake margin (fig. 6B and C). The differences observed between the sediment cores may relate to the presence of multiple or migrating influx point(s) along the subglacial lake cavity grounding line, as well as an interlinked palaeo-subglacial lake system. Underflows, in the form of debris or turbidity flows, are suggested to be a common depositional process within subglacial lakes (Bentley et al., 2011; Livingstone et al., 2012) and have been observed in other palaeo-subglacial lake records (e.g. Munro-Stasiuk, 2003; Christoffersen et al., 2008; Hodgson et al., 2009; Hodson et al., 2016; Kuhn et al., 2017).

Massive sandy-mud and sandy-silt inclusions in subunit 3c, together with occasional larger clasts, can be explained through a combination of rain-out from sediment-laden basal ice from the ceiling of a subglacial lake cavity and deposition from meltwater-derived underflows (fig. 6A), processes considered common in subglacial lakes (Siegert, 2000; Bentley et al., 2011;

Livingstone et al., 2012, 2015). Rain-out from the sediment-laden basal ice ceiling is likely to have been a significant process in this subglacial lake system, with the coarser patches and layers of sandy sediment such as those observed in core 1230 (figs. 4E and 5C), originating from proximity to the influx point of sediment laden (e.g. similar to that observed by Powell and Molnia, 1989, and Ó Cofaigh, 2007). There are few variations in shear strength in subunit 3c and this, in combination with its relatively homogeneous sedimentary structure, suggests that ice grounding events either did not occur in this basin or were not preserved in the sedimentary record. On the contrary, the coarse and consolidated nature of the winnowed till (subunit 3b) indicates that the pre-existing diamict has been winnowed by high bottom currents and may have experienced near-ice grounding events (fig. 4A).

While the presence of two high- to low-energy sequences (subunits 2c and 2b) might represent common drainage events within the basins and the presence of rain-out till (subunit 3c) indicates deposition from sediment-rich basal ice within closed subglacial-lake environments, the chloride pore water measurements do not indicate any freshwater signal (figs. 4A-E). The concentrations observed within all of the cores were of similar concentrations to seawater and so, we suggest that the sediments within these basins may have been deposited either within a subglacial lake near the ice margin or under an ice shelf cavity/proximal to the ice margin.

5.2 Hydrological variations within the subglacial lakes

Due to the size of these basins and their close proximity, it is unlikely that there were great differences in the overall level of hydrological activity, which we define here as the amount of meltwater draining into and out of these systems. However, differing levels of hydrological activity between the lower and upper basins were observed both in the glacial geomorphological and sedimentological records. The differences between these basins may also relate to switching of flow routing within this system.

Small meltwater channels link all of the basins together, indicating channelised drainage through this interconnected subglacial lake system. However, as aforementioned there are considerably more meltwater channels connecting into the middle and lower basin (figs. 2 and 3), suggesting greater hydrological activity within these palaeo-subglacial lakes. Alternatively the presence of several channels can also indicate migrating meltwater routing flow paths, caused due to variations in the meltwater input. The sedimentary records from the lower and middle basins also support increased hydrological activity and faster water currents, with the presence of clast-rich, winnowed till (subunit 3b). The winnowed till is considerably coarser than the rain-out till from the upper and margin of the middle basin cores, supporting sedimentation in an environment with fast water currents and periodic lake drainages.

The glacial geomorphology of the upper basin indicates more stable hydrological conditions with a singular feeder channel leading into it (fig. 3A and C). In support of this the sediments show little evidence for hydrological activity, but instead comprise a thick diamicton deposited by a combination of rain-out, current re-working and flow remobilization (fig. 4E). The core collected from the margin of the middle basin (core 1228) also displays a less hydrologically active depositional environment in contrast to the core from inside the middle basin (core 1225). We suggest that the sediments in this marginal area, similarly to the upper basin, may have either been better preserved due to the small ridges (~6 m high) downstream of the core extraction site or due to the fact that fast water velocities in the middle basin did not extend to its margin (fig. 3A).

It is important to take into consideration that while it is possible that the upper basin sedimentary record (core 1230) represents a less hydrologically active and marginal subglacial lake depositional setting, fast water currents may have also passed through this basin. Similar environments have been observed in West Antarctica, where a sediment record from Subglacial Lake Whillans, did not present much sedimentological variation, even though observations show that this subglacial lake undergoes floods, and cyclic periods of filling/drainage, as well as being part of an extensive and active subglacial hydrological system (Fricker et al., 2007; Hodson et al., 2016).

5. 3. Model for subglacial lake formation and activity on Thor Iversenbanken during the last glaciation

Subglacial hydraulic potential modelling in the Barents Sea suggests that the overlying ice geometry was favourable for the formation of subglacial lakes and focussed drainage routing through Thor Iversenbanken during the LGM (Shackleton et al., 2018). The formation of these subglacial lakes will have been influenced by their location in relation to: 1) the bank directly upstream, which allowed for a cavity to open on its lee-side; 2) the bathymetric highs, ridges, and banks surrounding the basins forming as areas of higher basal stress, which allowed for areas of low basal shear stress to form in between, enabling water to pond (e.g. Sergienko and Hindmarsh, 2013; Livingstone et al., 2016); and 3) their proximity to the shear margin, which would have promoted the generation of meltwater along this shear zone (e.g. Hulbe and Fahnestock, 2004; Perol et al., 2015). However, while this study cannot provide an exact time for channel and subglacial lake formation, we suggest that this palaeo-subglacial lake system may have been located close to the ice margin and active during the later-stages of deglaciation over Thor Iversenbanken. We favour this interpretation due to the observation of channels breaching of ice marginal deposits in the area and also the normal level of chloride concentrations in the sediment pore waters (figs. 2-4).

Shallow and transient subglacial lakes are likely to have formed within the small basins behind the ridges, periodically draining downstream through the channels cut into the sediment (figs. 2, 3 and 6A). Our observations are consistent other recent palaeo-subglacial lake discoveries in Canada and Antarctica (e.g. Livingstone et al., 2016; Kuhn et al., 2017; Simkins et al., 2017). These studies have shown that the lakes periodically drained and likely experienced cyclic filling and drainage events, similar to the cycles observed in contemporary subglacial lakes (e.g. Wingham et al., 2006; Smith et al., 2009; Palmer et al., 2013).

Meltwater at the bed of an ice mass can significantly alter the overlying ice flow velocity and dynamics (Gray et al., 2005; Fricker et al., 2007; Fricker and Scambos, 2009; Winsborrow et al., 2010b). Given the prominent location of these channels and basins at the margin between slow-flowing ice on Thor Iversenbanken and the Sentralbankrenna Ice Stream, it is likely they played a significant role in the ice flow dynamics of the ice stream. While the location of these palaeo-subglacial lakes is not near or at the onset zone of an ice stream, they may have drained into Sentralbankrenna prior to ice margin retreat of the ice stream further north-east, and would therefore have enhanced ice streaming by lubricating the bed and promoting sediment deformation (e.g. Bell, 2007; Winsborrow et al., 2010b). Changes in the water volumes draining into the trough will have promoted instabilities in Sentralbankrenna Ice Stream, potentially influencing ice stream flow switching farther downstream, such as those observed in Bjørnøyrenna (Piasecka et al 2016) and in the southwestern Barents Sea (Winsborrow et al., 2012).

It is uncertain whether the palaeo-subglacial lakes in the study area experienced full drainage, where the ice then reconnected with the ground. However, the presence of clast-rich, winnowed till with higher shear strengths (figs. 4B-C and 5B) in combination with the presence of numerous channels and tunnel valleys (figs. 2 and 3), strongly suggests that the study area underwent filling and partial drainage events (fig. 6A). During the rising limb of a drainage event, as subglacial meltwater entered the lake, the lake bed would have been winnowed and the deposition of finer materials inhibited. Whereas during the falling limb of a drainage events, water velocities would have decreased, allowing for the deposition of finer sediments. We suggest that the upper basin may have had calmer, less active hydrological conditions, enabling the deposition of a thick diamicton formed by the rain-out of sediment from the ice ceiling (fig. 6A).

While this area is likely to have been located near the ice margin and therefore influenced by marine waters and potentially tides, the sediments in subunit 2c are likely to have been deposited within a subglacial lake cavity. The sediment record indicates variation in hydrological activity within the basins, with a reorganisation of meltwater routing enabling the deposition of high- to low-energy depositional units (subunits 2b and 2c; fig. 5E and F). These were likely formed by turbidity flows originating from sediment-laden subglacial meltwater inflowing from subglacial channel(s) at the subglacial lake margin (fig. 6B), however there are uncertainties relating to the timing and exact position of the subglacial channel influx point(s) of meltwater draining into the lakes. The depositional environment of subunit 2b is more uncertain, although it likely represents deposition beneath an open-subglacial lake/ice shelf cavity at the grounding-zone of the ice margin (fig. 6C). This subunit, along with the glaciomarine subunit 2a, may have been influenced through the suspension settling of sediments from meltwater overflows and meltwater plumes (fig. 6B-D; e.g. Bentley et al., 2011; Livingstone et al., 2012; Dowdeswell et al., 2015), depositing the proximal to distal record we observe. The uppermost units we observed are characteristic of open-marine sedimentation (fig. 6E).

6. Conclusions

- On the northwestern flank of Thor Iversenbanken, central Barents Sea, three small basins are interpreted to have hosted palaeo-subglacial lakes interconnected by a network of meltwater channels.
- A suite of gravity cores were collected from the palaeo-subglacial lake basins and adjacent bank area.

- This study represents the first sedimentological evidence of palaeo-subglacial lake activity in the Barents Sea.
- The sediment record together with the geomorphological evidence, show clear indications for the presence of meltwater and differing levels of hydrological activity within the palaeo-subglacial lakes.
- The hydrologically active subglacial lakes are characterised by winnowed till associated with the presence of increased meltwater and switching of flow routing in the basin, during drainage events.
- The less hydrologically active subglacial lake is characterised by the preservation and deposition of a relatively homogeneous, massive diamict that represents rain-out of sediment from basal ice.
- The palaeo-subglacial lakes experienced a change in hydrological regime, characterised by the deposition of high- to low-energy sediment sequences with up-core fining. These successions are similar within all the basins. However, in the less hydrologically active subglacial lakes they are considerably coarser, indicating deposition nearer to the influx point at ice margin of the subglacial lake.
- These palaeo-subglacial lakes were likely formed along a shear margin zone between Sentralbankrenna Ice Stream and the slower bank area ice on Thor Iversenbanken, but proximal to the ice margin of Thor Iversenbanken.
- While these palaeo-subglacial lakes are likely to have been relatively shallow (<20 m), they were transient and hydrologically dynamic features within the subglacial hydrological system on Thor Iversenbanken and may have significantly influenced the ice flow velocities of Sentralbankrenna Ice Stream.

Acknowledgements

We would like to acknowledge the Norwegian Hydrographic Service and the MAREANO programme for the collection and provision of this dataset. This work was by the Research Council of Norway through its Centres' of Excellence funding scheme, project number 223259, to the Research Centre for Arctic Gas Hydrate, Environment and Climate (CAGE). We would like to thank the captain and crew of R/V Helmer Hanssen, participants of the 2015 cruise, and Diane Groot for their contributions during data collection. In addition, we would like to thank Jan Piotrowski, Sarah Greenwood and Timothy Hodson for their constructive comments to the

manuscript during the peer-review process following the submission of this paper to Boreas in 2018.

Figures and tables

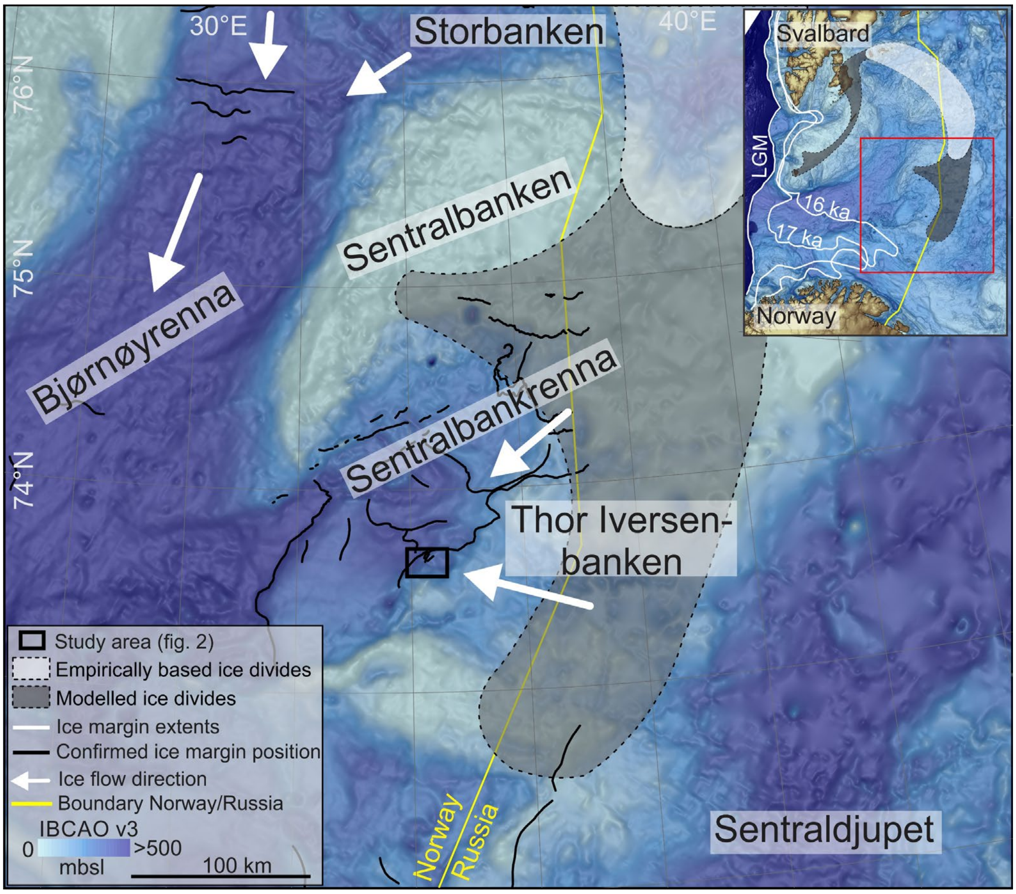

Figure 1. Map of the central Barents Sea showing the location of the study area, marine border between Norway and Russia, ice flow directions of BSIS, as well as, the Storbanken ice divide (Bondevik et al., 1995; Ottesen et al., 2005) and its modelled extent over Sentralbanken/Spitsbergenbanken (Patton et al., 2015). Empirically based confirmed ice margin positions (Rüther et al., 2012; Andreassen et al., 2014; Bjarnadottir et al., 2014; Esteves et al., 2017). Inset map shows the BSIS ice margin extents during the LGM (Svendsen et al., 2004), and 17- and 16-cal ka BP (Winsborrow et al., 2010; Hughes et al., 2016), as well as the

full extent of the ice divide. The Bathymetric Chart of the Arctic Ocean (IBCAO) version 3.0. was used for the background bathymetry (Jakobsson et al., 2012).

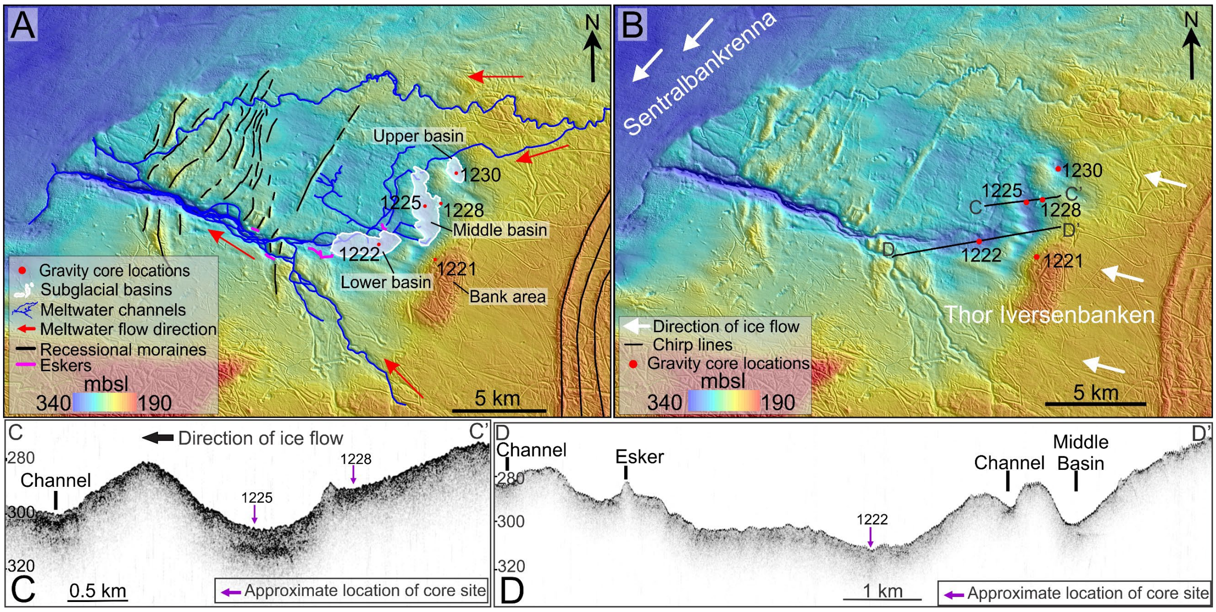

Figure 2. Overview of study area on northwestern flank of Thor Iversenbanken. A) Glacial geomorphological mapping (modified from Esteves et al., 2017) and location of the gravity core sites. B) High resolution bathymetry of the palaeo-subglacial basins on Thor Iversenbanken with the location of chirp lines and gravity core collection site. C) Cross profile of the middle basin. D) Long profile of the southern basin. Multibeam bathymetry: © Kartverket.

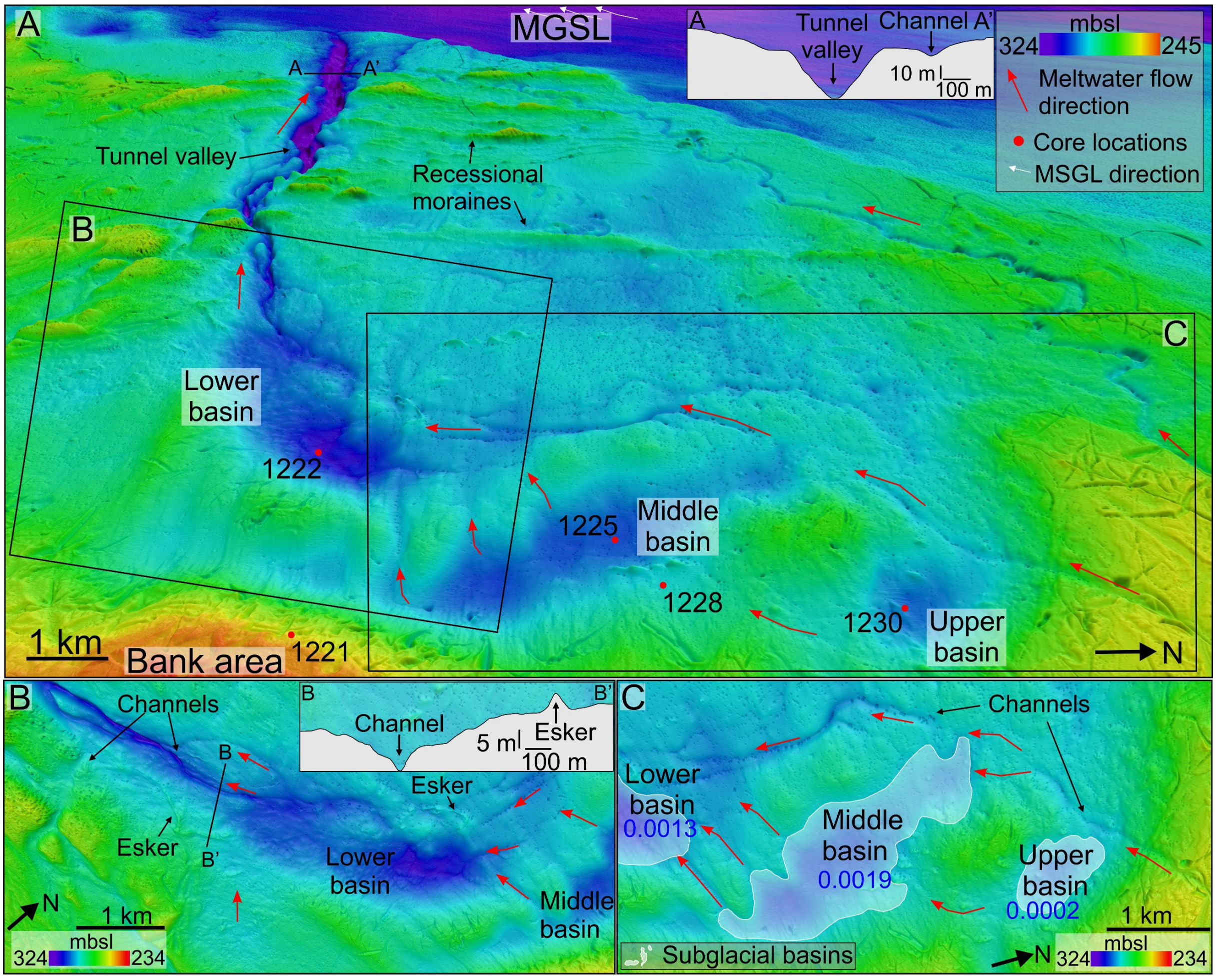

Figure 3. Interconnected palaeo-subglacial lake system. A) Meltwater channels connect all three basins before forming dendritic system and large tunnel valley that leads into the trough, Sentralbankrenna, where large mega-scale glacial lineations (MSGL) can be observed. Inset profile shows cross sectional profile of the tunnel valley. B) Close-up of the lower basin with the inflow and outflow channels and eskers. Inset profile shows cross section of an esker and the channel that evolves into the tunnel valley. C) Inflow and outflow channels for the upper and middle basin, as well as the volume capacities (km^3) for the mapped basin extents for all three basins (for the full mapping of basins and other glacial landforms, cf. figure 2A). Multibeam bathymetry: © Kartverket.

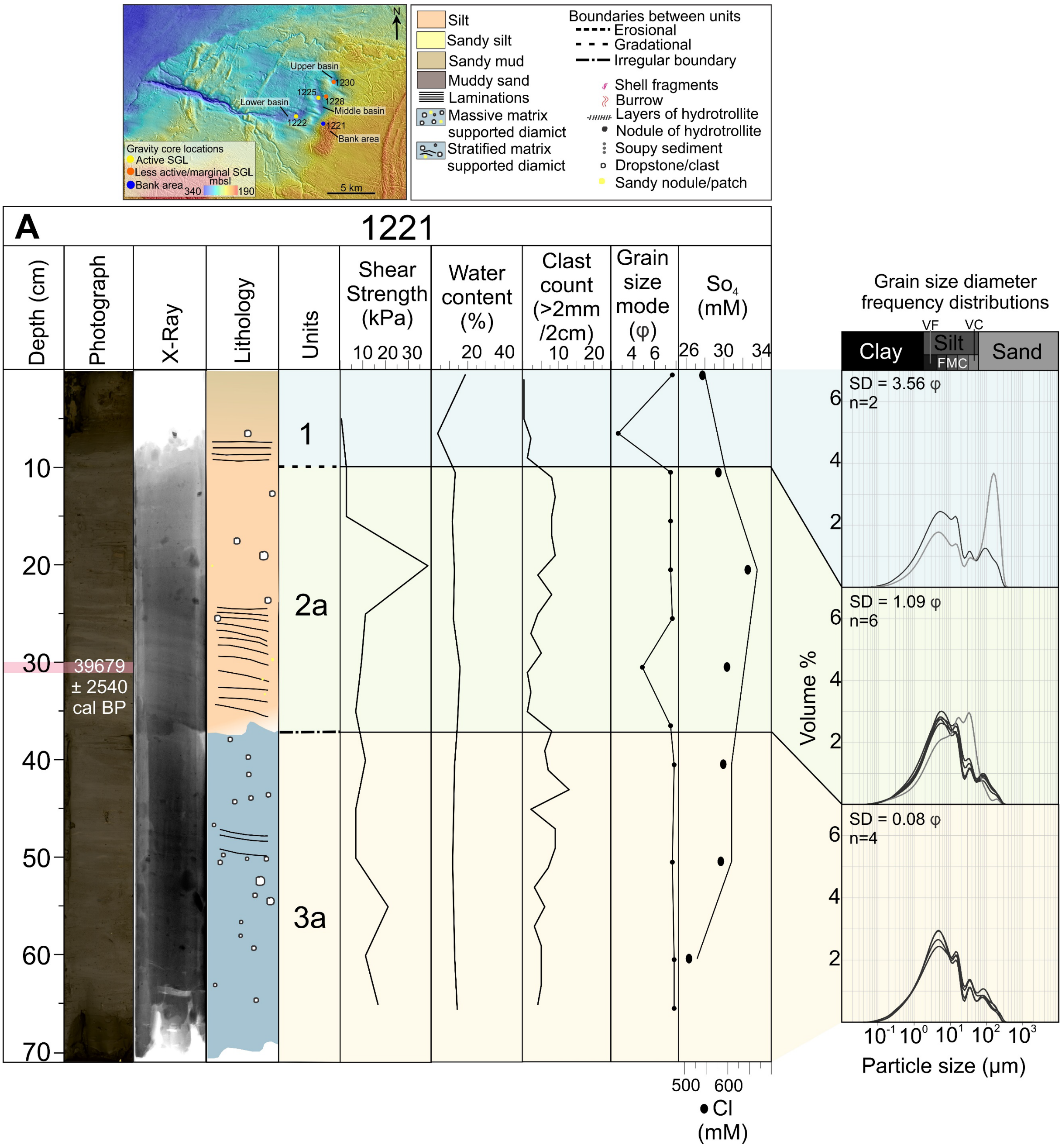
Upper basin
Lower basin
Middle basin
Bank area
1230
1225
1228
1222
1221
Gravity core locations
Active SGL
Less active/marginal SGL
Bank area
mbsl
340
190
5 km
Silt
Sandy silt
Sandy mud
Muddy sand
Laminations
Massive matrix supported diamict
Stratified matrix supported diamict
Boundaries between units
Erosional
Gradational
Irregular boundary
Shell fragments
Burrow
Layers of hydrotrollite
Nodule of hydrotrollite
Soupy sediment
Dropstone/clast
Sandy nodule/patch
A
1221
Depth (cm)
Photograph
X-Ray
Lithology
Units
Shear Strength (kPa)
Water content (%)
Clast count (>2mm /2cm)
Grain size mode (φ)
So4 (mM)
39679 ± 2540 cal BP
1
2a
3a
500 600
● Cl (mM)
Grain size diameter frequency distributions
Clay
Silt
Sand
VF
VC
FMC
SD = 3.56 φ
n=2
SD = 1.09 φ
n=6
SD = 0.08 φ
n=4
Volume %
Particle size (μm)

594

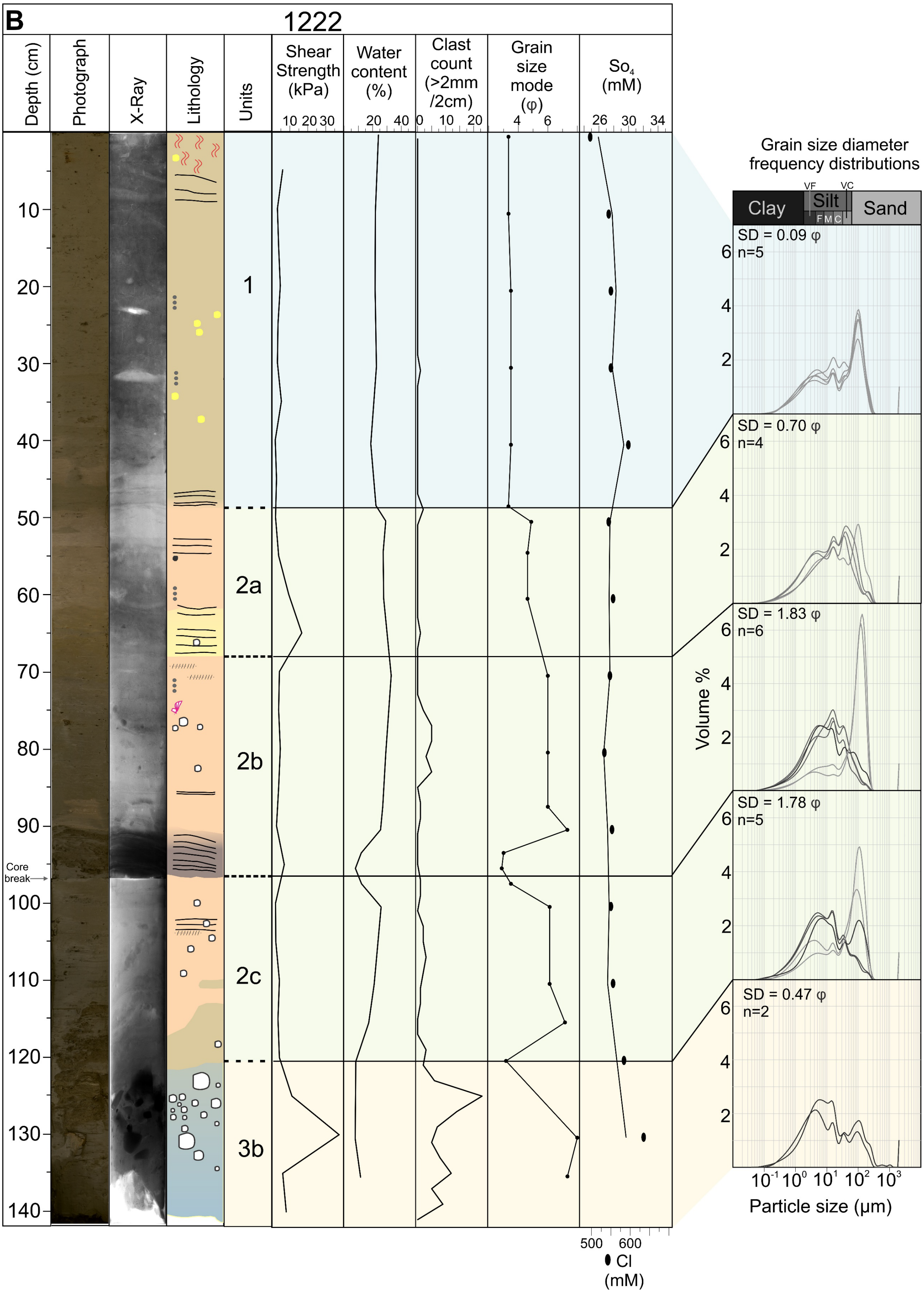
B
1222
Depth (cm)
Photograph
X-Ray
Lithology
Units
Shear Strength (kPa)
10 20 30
Water content (%)
20 40
Clast count (>2mm /2cm)
0 10 20
Grain size mode (φ)
4 6
So4 (mM)
26 30 34
10
20
30
40
50
60
70
80
90
Core break
100
110
120
130
140
1
2a
2b
2c
3b
500 600
Cl (mM)
Grain size diameter frequency distributions
Clay
Silt
VF VC
F M C
Sand
SD = 0.09 φ
n=5
SD = 0.70 φ
n=4
SD = 1.83 φ
n=6
SD = 1.78 φ
n=5
SD = 0.47 φ
n=2
6
4
2
Volume %
Particle size (µm)

595

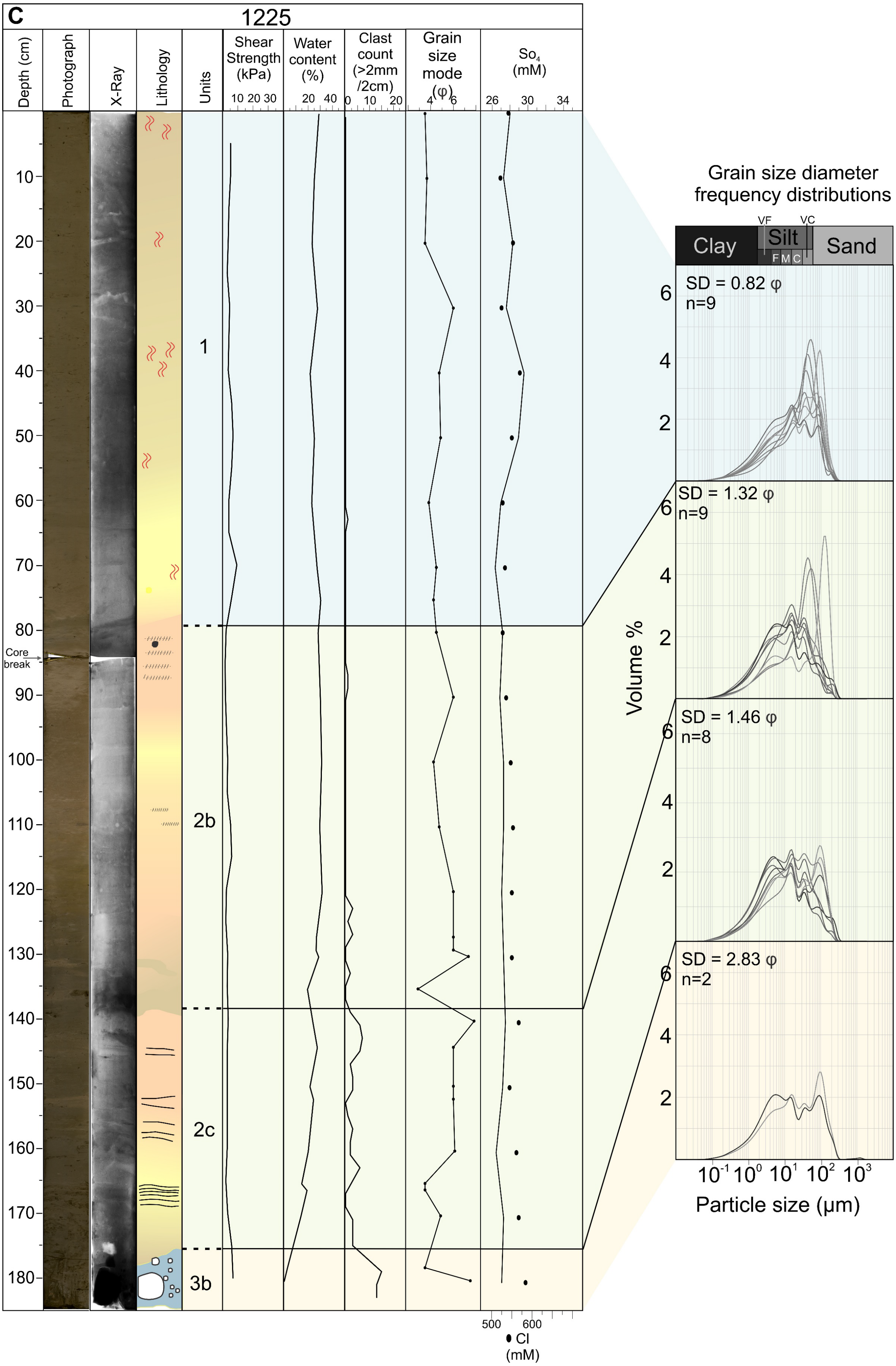
C
1225
Depth (cm)
Photograph
X-Ray
Lithology
Units
Shear Strength (kPa)
Water content (%)
Clast count (>2mm /2cm)
Grain size mode (φ)
So4 (mM)
1
2b
2c
3b
Core break
Cl (mM)
Grain size diameter frequency distributions
Clay
Silt
Sand
VF
VC
F M C
SD = 0.82 φ
n=9
SD = 1.32 φ
n=9
SD = 1.46 φ
n=8
SD = 2.83 φ
n=2
Volume %
Particle size (μm)

596

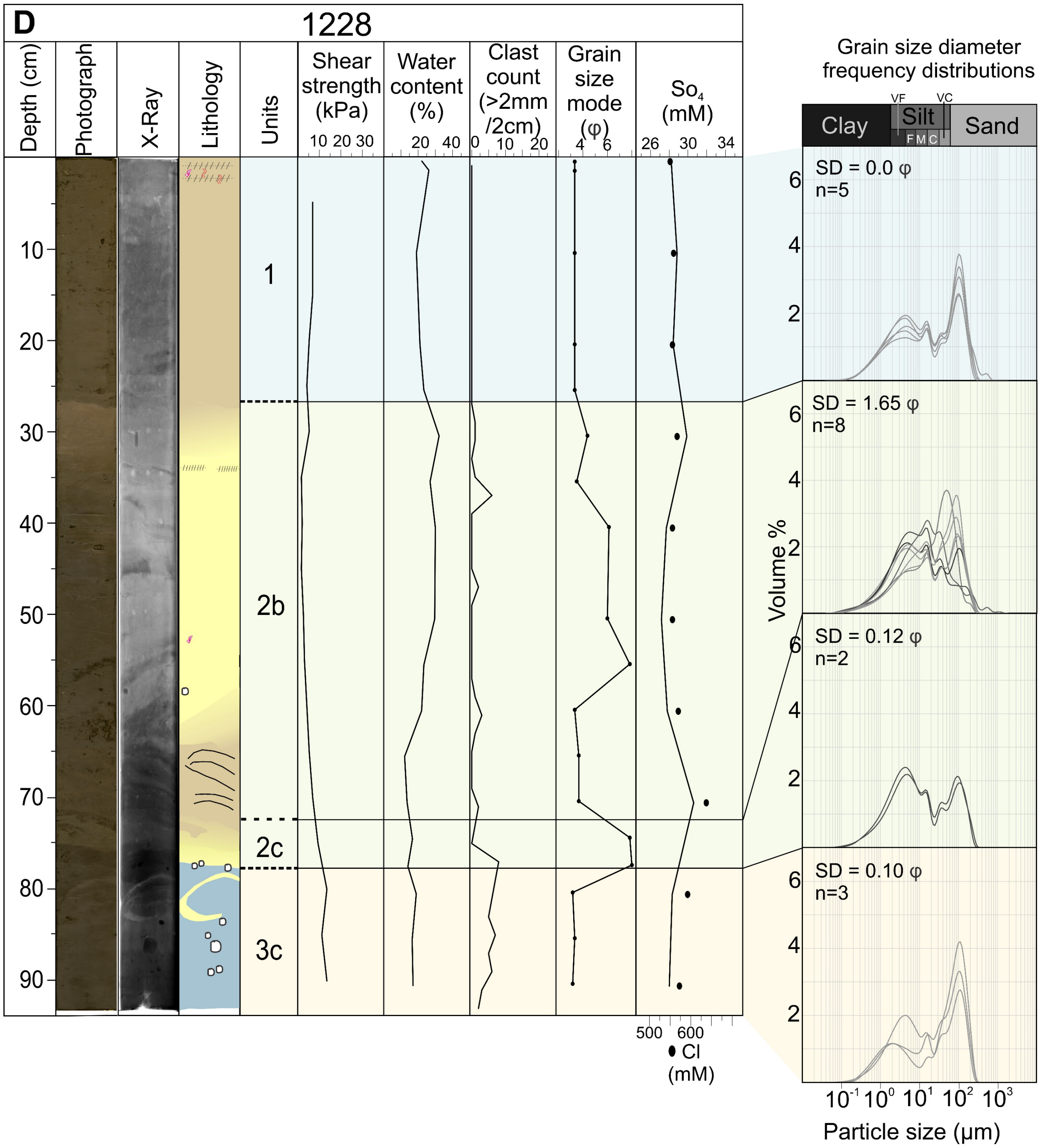
D
1228
Depth (cm)
Photograph
X-Ray
Lithology
Units
Shear strength (kPa)
10 20 30
Water content (%)
20 40
Clast count (>2mm /2cm)
0 10 20
Grain size mode (φ)
4 6
So4 (mM)
26 30 34
1
2b
2c
3c
10
20
30
40
50
60
70
80
90
500 600
Cl (mM)
Grain size diameter frequency distributions
Clay
Silt
VF VC
F M C
Sand
SD = 0.0 φ
n=5
SD = 1.65 φ
n=8
SD = 0.12 φ
n=2
SD = 0.10 φ
n=3
Volume %
Particle size (µm)

597

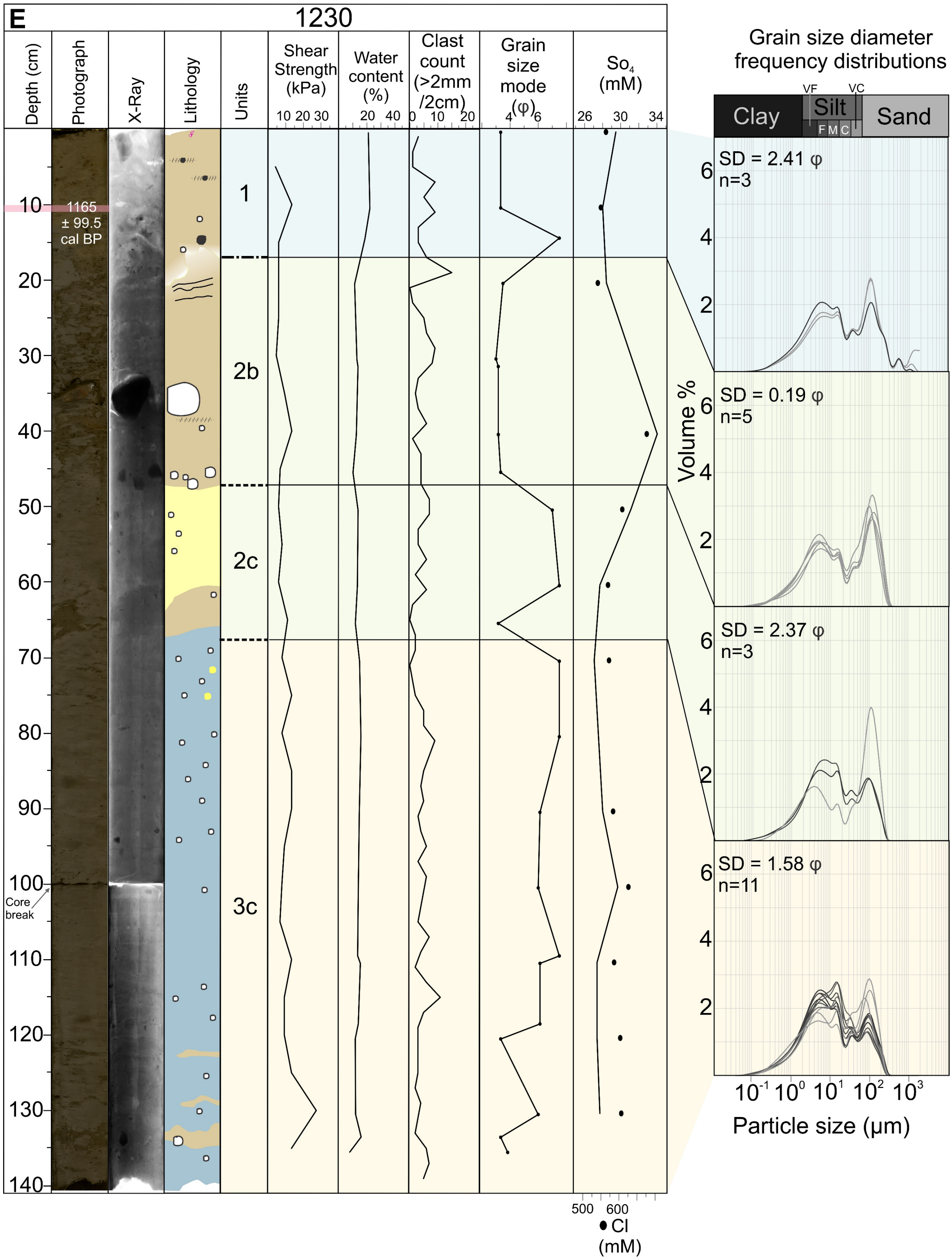

Figure 4. Overview of all cores and their sedimentological, physical and geochemical properties, from left to right: high-resolution photograph, x-radiograph, lithology, interpreted units, shear strength, water content, clast counts, grain size mode, chloride (black dots) and sulphide (solid line) pore water concentrations, and representative grain size diameter

frequency distributions for each unit (Wentworth grain-size classifications are used and denoted above; SD = Standard deviation of phi; N = number of samples per unit). A) Core 1221, recovered from the lee-side of the bank area. B) Core 1222, recovered from inside the southern basin directly upstream of the tunnel valley. C) Core 1225, recovered from inside the middle basin. D) Core 1228, recovered from the margin of the middle basin. E) Core 1230, recovered from inside the northern basin in the area. Inset map shows core locations and their interpretation as either bank, active subglacial lake or calm/marginal subglacial lake. SGL – subglacial lake. Multibeam bathymetry: © Kartverket.

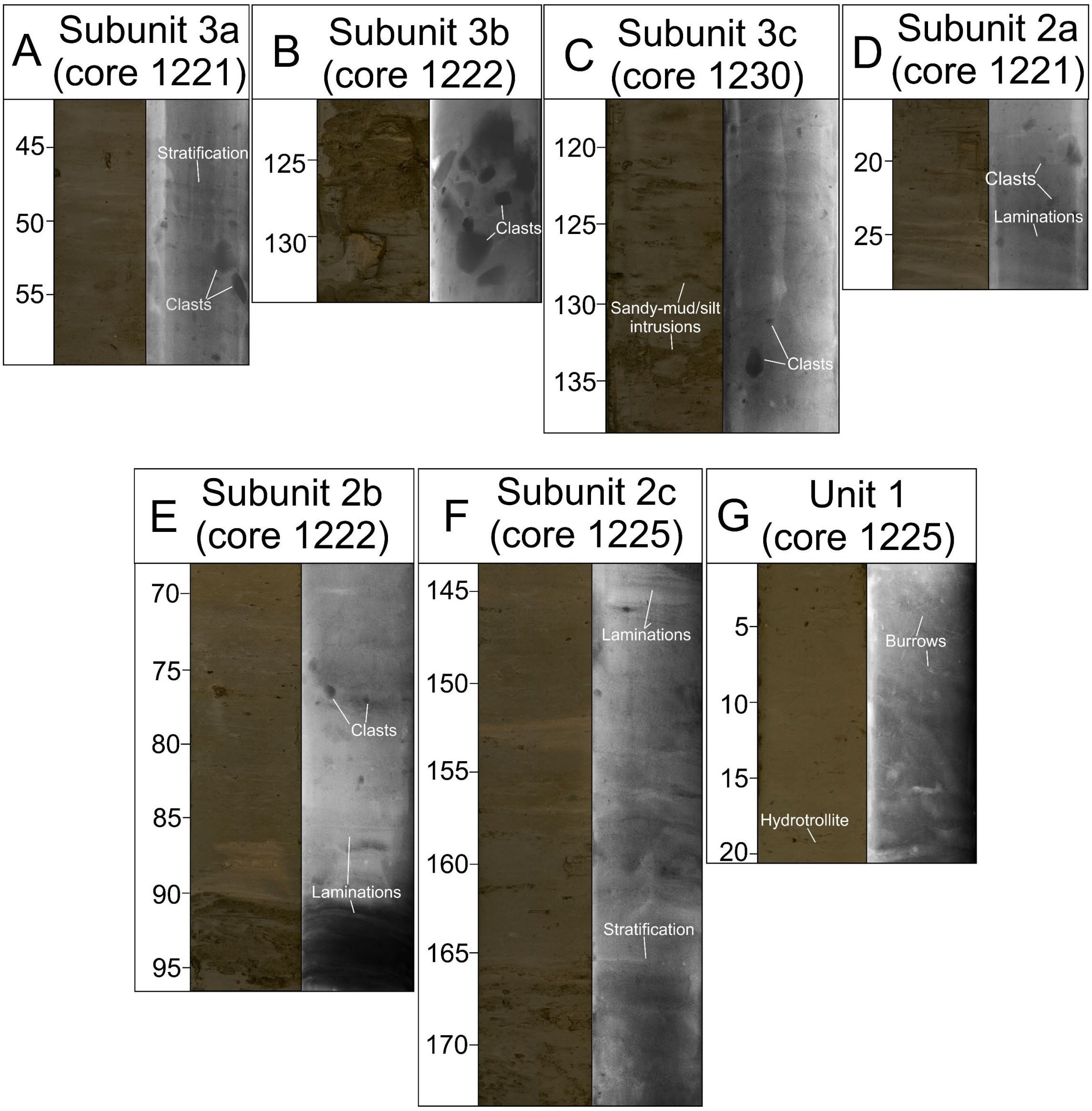

Figure 5. High resolution photographs and x-radiographs of the key facies and features for each of the units. A) Subunit 3a displays a relatively homogenous matrix with clasts interspersed and a small crudely stratified section. B) Subunit 3b is a clast supported matrix. C) Subunit 3c is characterised by its relatively homogenous, massive matrix with several patches of sandy

mud and interspersed clasts. D) Subunit 2a has a laminated sandy-silt interval that transitions up-core to a homogenous silt matrix, interspersed with occasional clasts. E) Subunit 2b is the second and shallowest high- to low-energy deposition sequence, composed of several sandy mud/silt laminations at the base and shell fragments and hydrotrollites at the top of the unit. F) Subunit 2c has an up-core fining sequence with coarse stratifications at the base of the unit and laminations within the fining transition. G) Unit 1 shows increased bioturbation, burrows and hydrotrollites.

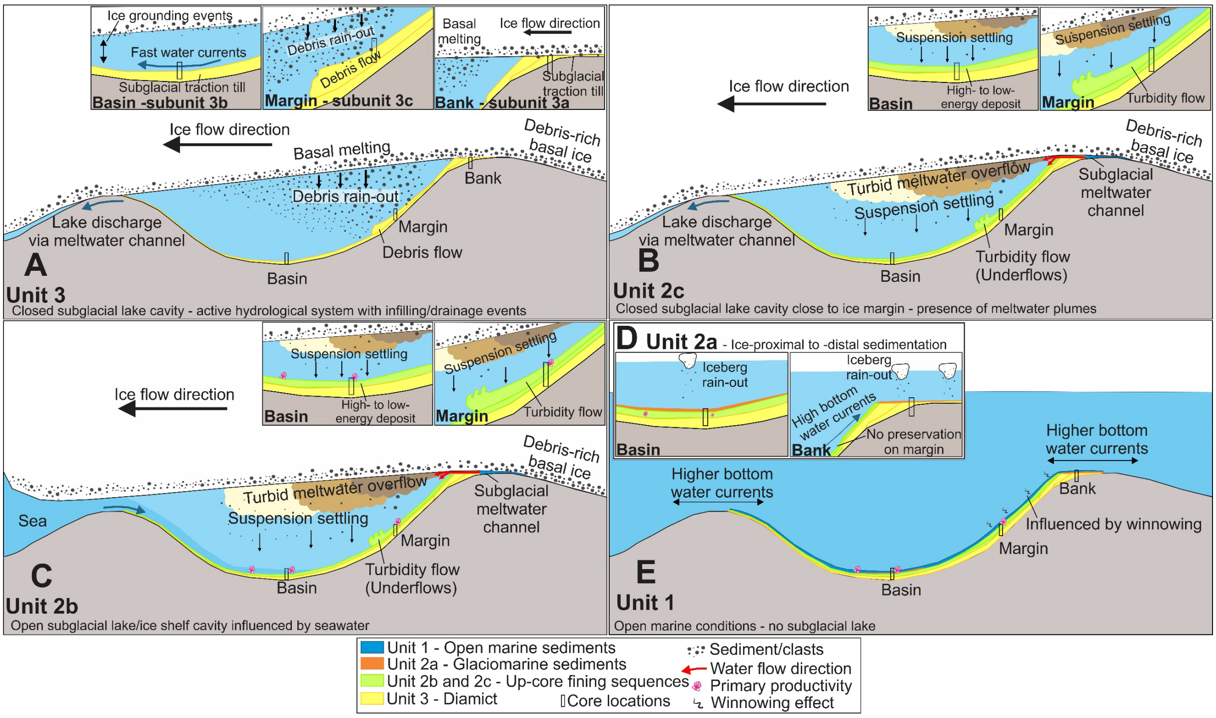

Figure 6. Simplified conceptual model showing the overall reconstructed subglacial processes occurring within subglacial lakes on Thor Iversenbanken, with a particular focus on the depositional environments for units 1-3 inside the basin (cores 1222 and 1228), at the margin (cores 1225 and 1230), and on the lee-side of the bank (core 1221). A) Unit 3 was deposited within a closed subglacial lake cavity under active subglacial hydrological conditions that experienced infilling and drainage events. Insets show the different processes occurring at each of the areas and the related subunits. B) Unit 2c represents high to low energy deposition from meltwater plumes and suspension settling within a closed subglacial lake close to the ice margin. C) Unit 2b represents the second high to low energy depositional environment similar to subunit 2c, however with an increased presence of primary productivity indicating an open subglacial lake or ice shelf cavity near the ice margin that is influenced by seawater. D) Unit 2a represents typical ice-proximal to –distal deposition of glaciomarine sediments with some interspersed clasts from iceberg rain-out. E) Unit 1 represents open marine sedimentation.

Table 1. Overview of sediment gravity cores in this study. Basins shown in figures 2 and 3.

Core ID	Referred to in this study as	Latitude (N)	Longitude (E)	Water Depth (m)	Recovery (m)	Location in relation to landforms (c.f. fig. 2)
CAGE15-5-1221-GC	1221	73°36.590’	34°41.446’	253	0.72	Bank area
CAGE15-5-1222-GC	1222	73°37.042’	34°36.065’	310	1.41	Lower basin
CAGE15-5-1225-GC	1225	73°38.048’	34°40.612’	305	1.85	Middle basin
CAGE15-5-1228-GC	1228	73°38.107’	34°42.156’	291	0.94	Middle basin margin
CAGE15-5-1230-GC	1230	73°38.918’	34°43.722’	300	1.4	Upper basin

Table 2. The uncorrected and calibrated radiocarbon dates (mean probability; 1σ range; 2σ range) presented in this study.

Core name and sample depth	Litho-facies unit	Material	Radiocarbon age (14C BP)	Calibrated age (cal BP)	1σ range	2σ range	Lab ID
1221 30-31 cm	2a	Bulk foraminifera	35700±1200	39679	38559-41088	36853-41933	Poz-90724
1230 10-11 cm	1	Bulk foraminifera	1670±35	1165	1116-1226	1057-1256	Poz-90445

Table 3. Overview of the units based on their lithology, physical properties and observed structures.

Unit (colour)	Sub-unit (fig.)	Cores	Unit thickness (cm)	Lithological characteristics	Shear Strength av. (kPa)	Water content av. (%)	Lower unit boundaries	Depositional environment
1 (Dark grey to olive grey/green-brown)	- (fig. 5G)	All cores	10-79.5	Silt to sandy-silt or sandy-mud. Shell fragments, hydrotrollites and burrows.	5.17	20.30	Gradational (1221; 1222; 1225) Erosional (1228) Irregular boundary (1230)	Open marine
2 (Dark grey to dark olive-brown)	2a (fig. 5D)	1221; 1222	19-27	Laminations of silty and sandy-silt to homogeneous silt. No indications of shells or burrows.	7.75	20.64	Irregular boundary (loaded; 1221) Erosional (1222)	Glaciomarine
	2b (fig. 5E)	1222; 1225; 1228; 1230	28.5-59	Muddy sand and sandy-mud to silt and sandy-silt. Up-core fining sequence. Coarse laminations at the base. Shell fragments, and hydrotrollites.	4.64	21.58	Erosional (1222; 1230) Gradational (1225; 1228)	Open subglacial cavity near ice margin influenced by marine waters.
	2c (fig. 5F)	1222; 1225; 1228; 1230	5.5-37	Sandy-mud/ sandy-silt to sandy-silt/silt. Up-core fining sequence. Laminations within the fining transition. No indications of shells or burrows.	5.94	16.52	Erosional (1228; 1230), gradational (1222; 1225)	Subglacial lake. Change from active to calm hydrological conditions. Indications for meltwater plumes.
3 (Very dark to dark grey)	3a (fig. 5A)	1221	34	Matrix supported diamict with some crude stratification.	12.31	12.87	Base of core	Subglacial traction till.
	3b (fig. 5B)	1222; 1225	9.5-21	Massive matrix-clast supported diamict with several large clasts.	11.27	5.72	Base of core	Subglacial lake. Winnowed till.
	3c (fig. 5C)	1228; 1230	16-73.5	Massive matrix supported diamict with few large clasts. Several layers/patches of sandy-mud and sandy-silt.	12.34	15.63	Base of core	Subglacial lake. Rain-out till.

References

Alley, R. B., Blankenship, D. D., Bentley, C. R., Rooney, S. T., 1986. Deformation of till beneath ice stream B, West Antarctica. Nature 322, 57–59.

Alley, R.B., Anandakrishnan, S., Bentley, C.R., Lord, N., 1994. A water-piracy hypothesis for the stagnation of Ice Stream C, Antarctica: Ann. Glaciol. 20, 187–194.

Andreassen, K.A., Nilssen, L.C., Rafaelsen, B., Kuilman, L., 2004. Three-dimensional seismic data from the Barents Sea margin reveal evidence of past ice streams and their dynamics. Geology 32 (8), 729–732.

Andreassen, K., Laberg, J.S., Vorren, T.O., 2008. Sea floor geomorphology of the SW Barents Sea and its glaci-dynamic implications. Geomorphology 97 (1-2), 157-177.

Andreassen, K., Winsborrow, M., Bjarnadóttir, L. R., Rüther, D. C., 2014. Ice stream retreat dynamics inferred from an assemblage of landforms in the northern Barents Sea. Quat. Sci. Rev., 92, 246–257.

Andreassen, K., Winsborrow, M.C.M., 2009. Signature of ice streaming in Bjørnøyrenna, Polar North Atlantic through the Pleistocene and implications for ice stream dynamics. Ann. Glaciol. 50 (52), 17 – 26.

Andrews, L. C. Catania, G. A., Hoffman, M. J., Gulley, J. D., Lüthi, M.P., Ryser, C., Hawley, R. L., Neumann, T. A., 2014. Direct observations of evolving subglacial drainage beneath the Greenland Ice Sheet. Nature 514, 80-83.

Bartholomew, I., Nienow, P., Mair, D., Hubbard, A., King, M. A., Sole, A., 2010. Seasonal evolution of subglacial drainage and acceleration in a Greenland outlet glacier. Nat. Geosci. 3, 408-411.

Bell, R. E., 2008. The role of subglacial water in ice-sheet mass balance. Nat. Geosci., 1, 297–304.

Bell, R. E., Tinto, K., Das, I., Wolovick, M., Chu, W., Creyts, T. T., Frearson, N., Abdi, A., Paden, J. D., 2014. Deformation, warming and softening of Greenland's ice by refreezing meltwater. Nat. Geosci. 7, 497–502.

Bentley, M. J., Christoffersen, P., Hodgson, D. A., Smith, A. M., Tulaczyk, S., Le Brocq, A. M., 2011. Subglacial Lake Sediments and Sedimentary Processes: Potential Archives of Ice Sheet Evolution, Past Environmental change and the Presence of Life. Antarctic Subglacial Aquatic Environments, Geophysical Monograph Series, 192, 83 – 110.

Bjarnadóttir, L.R., Winsborrow, M.C.M., Andreassen, K., 2014. Deglaciation of the central Barents Sea. Quat. Sci. Rev. 92, 208-226.

Bjarnadóttir, L.R., Winsborrow, M.C.M., Andreassen, K., 2017. Large subglacial meltwater features in the central Barents Sea. Geology 45 (2), 159–162.

Bondevik, S., J. Mangerud, L. Ronnert, O. Salvigsen., 1995. Postglacial sea-level history of Edgeøya and Barentsøya, eastern Svalbard. Polar Res. 14 (2), 153–180.

Bougamont, M., Tulaczyk, S., Joughin, I.R., 2003. Numerical investigations of the slow-down of Whillans Ice Stream, West Antarctica: is it shutting down like Ice Stream C? Ann. Glaciol. 37, 239–246.

Bouma, A. H., 1962. Sedimentology of Some Flysch Deposits: A Graphic Approach to Facies Interpretation, 168 pp., Elsevier, Amsterdam, Netherlands.

Christoffersen, P., Tulaczyk, S., Wattrus, N.J., Peterson, J., Quintana-Krupinski, N., Clark, C.D., and Sjunneskog, C., 2008. Large subglacial lake beneath the Laurentide Ice Sheet inferred from sedimentary sequences. Geology 36, 563 – 566.

Dowdeswell, J.A., Hogan, K.A., Arnold, N.S., Mugford, R.I.,Wells, M., Hirst, J.P.P., Decalf, C., 2015. Sediment-rich meltwater plumes and ice-proximal fans at the margins of modern and ancient tidewater glaciers: observations and modelling. Sedimentology, 62, 1665-1692.

Engelhardt, H., Kamb, B., 1997. Basal hydraulic system of a West Antarctic ice stream: constraints from borehole observations. Journal of Glaciology, 43, 207–231

Esteves, M., Bjarnadóttir, L.R., Winsborrow, M.C.M., Shackleton, C.S., Andreassen, K., 2017. Retreat patterns and dynamics of the Sentralbankrenna glacial system, central Barents Sea. Quat. Sci. Rev. 169, 131-147.

Elverhøi, A., Pfirman, S.L., Solheim, A., Larssen, B.B., 1989. Glaciomarine sedimentation in epicontinental seas exemplified by the northern Barents Sea. Marine Geology, 85, 225–250.

Elverhøi, A., Fjeldskaar, W., Solheim, A., Nyland Berg, M., Russwurm, L., 1993. The Barents Sea ice sheet – a model of its growth and decay during the last ice maximum. Quat. Sci. Rev. 12, 863–873.

Elverhøi A. & Solheim A. 1983. The Barents Sea ice sheet—a sedimentological discussion. Polar Research 1, 23–42.

Evans, J., Pudsey, C.J., 2002. Sedimentation associated with Antarctic Peninsula ice shelves: implications for palaeoenvironmental reconstructions of glacimarine sediments. J. Geol. Soc. Lond. 159, 233–237.

Evans, D. J. A., Rea, B. R., Hiemstra, J. F., and Ó Cofaigh, C., 2006. A critical assessment of subglacial mega-floods: a case study of glacial sediments and landforms in south-central Alberta, Canada. Quaternary Science Reviews, 25, 1638 – 1667.

Friedman, G.M., Sanders J.E., 1978. Principles of Sedimentology. John Wiley: New York.

Fricker, H. A., Scambos, T., Bindschadler, R., Padman, L., 2007. An active subglacial water system in West Antarctica mapped from space. Science, 315, 1544 – 1548.

Fricker, H. A., and Scambos, T., 2009. Connected subglacial lake activity on lower Mercer and Whillans Ice Streams, West Antarctica, 2003 – 2008. Journal of Glaciology 55 (190), 303 – 315.

Gray, L., Joughin, I., Tulaczyk, S., Spikes, V. B., Bindschadler, R., Jezek, K., 2005. Evidence for subglacial water transport in the West Antarctica Ice Sheet through three-dimensional satellite radar interferometry. Geophysical Research Letters, 32, L03501, doi: 10.1029/2004GL021387.

Grobe, H., 1987. A simple method for the determination of ice-rafted debris in sediment cores. Polarforschung, 57, 123–126.

Hansbo, S., 1957. A new approach to the determination of the shear strength of clay by the fall-cone test. Royal Swedish geotechnical Institute: Stockholm.

Hodson, T.O., Powell, R.D., Brachfeld, S.A., Tulaczyk, S., Scherer, R.P., Team WS., 2016. Physical processes in Subglacial Lake Whillans, West Antarctica: inferences from sediment cores. Earth and Planetary Science Letters, 444, 56–63.

Hodgson, D.A., Roberts, S.J., Bentley, M.J., Carmichael, E.L., Smith, J.A., Verleyen, E., Vyverman, W., Geissler, P., Leng, M.J., Sanderson, D.C.W., 2009. Exploring former subglacial Hodgson Lake, Antarctica Paper II: palaeolimnology. Quat. Sci. Rev. 28, 2310-2325.

Hooke, R. L., Iverson, N. R., 1995. Grain-size distribution in deforming subglacial tills: role of grain fracture. Geology 23, 57–60.

Hughes, A.L.C., Gyllencreutz, R., Lohne, Ø.S., Mangerud, J., Svendsen, J.I., 2016. The last Eurasian ice sheets - a chronological database and time-slice reconstruction, DATED-1. Boreas, 45, 1–45.

Hulbe, C. L., Fahnestock, M. A. 2004. West Antarctic ice-stream discharge variability: mechanism controls and pattern of grounding-line retreat. J. Glaciol. 50 (171), 471-484.

Jakobsson, M., Mayer, L., Coakley, B., Dowdeswell, J.A., Forbes, S., Fridman, B., Hodnesdal, H., Noormets, R., Pedersen, R., Rebesco, M., Schenke, H.W., Zarayskaya, Y., Accettella, D., Armstrong, A., Anderson, R.M., Bienhoff, P., Camerlenghi, A., Church, I., Edwards, M., Gardner, J.V., Hall, J.K., Hell, B., Hestvik, O.B., Kristoffersen, Y., Marcussen, C., Mohammad, R., Mosher, D., Nghiem, S.V., Pedrosa, M.T., Travaglini, P.G., Weatherall, P., 2012. The International Bathymetric Chart of the Arctic Ocean (IBCAO) Version 3.0. Geophys. Res. Lett. 39, LI2609.

Kapitsa, A., Ridley, J.K., Robin, G. de Q., Siegert, M.J., Zotikov, I., 1996. Large deep freshwater lake beneath the ice of central East Antarctica. Nature 381, 684–686

Kuhn, G. Hillenbrand, C-D., Kasten, S., Smith, J.A., Nitsche, F.O., Frederichs, T., Wiers, S., Ehrmann, W., Klages, J.P., Mogollón, J.M., 2017. Evidence for a palaeo-subglacial lake on the Antarctic continental shelf. Nat. Comms. 8:15591,1-10.

Landvik, J.Y., Bondevik, S., Elverhøi, A., Fjeldskaar, W., Mangerud, J., Salvigsen, O., Siegert, M.J., Svendsen, J.-I., Vorren, T.O., 1998. The last glacial maximum of Svalbard and the Barents Sea area: Ice sheet extent and configuration. Quat. Sci. Rev. 17, 43–75.

Livingstone, S. J., Clark, C. D., Piotrowski, J. A., Tranter, M., Bentley, M. J., Hodson, A., Swift, D. A., and Woodward, J., 2012. Theoretical framework and diagnostic criteria for the identification of palaeo-subglacial lakes. Quat. Sci. Rev. 53, 88 – 110.

Livingstone, S.J., Clark, C.D., Tarasov, L., 2013a. Modelling North American palaeo-subglacial lakes and their meltwater drainage pathways. Earth Planet. Sci. Lett. 375, 13–33. doi:10.1016/j.epsl.2013.04.017

Livingstone, S.J., Clark, C.D., Woodward, J., 2013b. Predicting subglacial lakes and meltwater drainage pathways beneath the Antarctic and Greenland ice sheets. The Cryosphere Discuss, 7, 1177-1213.

Livingstone, S. J., Piotrowski, J. A., Batemen, M. D., Ely, J. C., Clark, C. D., 2015. Discriminating between subglacial and proglacial lake sediments: an example from the Dänischer Wohld Peninsula, northern Germany. Quat. Sci. Rev. 112, 86-108.

Livingstone, S. J., Utting, D. J., Ruffell, A., Clark, C. D., Pawley, S., Atkinson, N., Fowler, A. C., 2016. Discovery of relic subglacial lakes and their geometry and mechanism of drainage. Nat. Commun., 7:11767.

Loeng, H., 1983. Strømmålinger i tidsrommet 1979–982 i de sentrale deter av Barentshavet. In Environmental Conditions in the Barents Sea and Near Jan Mayen, Eide LI (ed.). Institute of Marine Research: Bergen.

Loeng, H., 1991. Features of the physical oceanographic conditions of the Barents Sea, Polar Res., 10, 5–18.

Mangerud, J., Bondevik, S., Gulliksen, S., Hufthammer, A. K., Høisæter, T., 2006. Marine 14C reservoir ages for 19th century whales and molluscs from the North Atlantic, Quaternary Sci. Rev., 25, 3228–3245.

McCabe, A. M., Ó Cofaigh, C. 1994. Sedimentation in subglacial lake, Enniskerry, eastern Ireland. Sedimentary Geology 91, 57-95.

Munro-Stasiuk, M.J., 2003. Subglacial Lake McGregor, south-central Alberta, Canada. Sedimentary Geology, 160, 325 – 350.

Newton, A.M.W., Huuse, M., 2017. Glacial geomorphology of the central Barents Sea: Implications for the dynamic deglaciation of the Barents Sea Ice Sheet. Mar. Geol. 387, 114–131.

Ó Cofaigh, C., Evans, J., Dowdeswell, J.A., Larter, R. D., 2007. Till characteristics, genesis and transport beneath Antarctic paleo-ice streams. Journal of Geophysical Research, 112: F03006.

Oswald, G.K.A., Robin, G. de Q., 1973. Lakes beneath the Antarctic ice sheet. Nature 275, 251–254.

Ottesen, D., Dowdeswell, J.A., Rise, L., 2005. Submarine landforms and the reconstruction of fast-flowing ice streams within a large Quaternary ice sheet: The 2500-km-long Norwegian-Svalbard margin (57-80N). GSA Bulletin. 117, 1033–1050.

Palmer, S. J., Dowdeswell, J. A., Christoffersen, P., Young, D. A., Blankenship, D. D., Greenbaum, J. S., Benham, T., Bamber, J., and Siegert, M. J., 2013. Greenland subglacial lakes detected by radar. Geophysical Research Letters, 40, 6154 – 6159.

Patton, H., Andreassen, K., Bjarnadóttir, L.R., Dowdeswell, J.A., Winsborrow, M.C.M., Noormets, R., Polyak, L., Auriac, A., Hubbard, A., 2015. Geophysical constraints on the dynamics and retreat of the Barents Sea Ice Sheet as a palaeo-benchmark for models of marine ice-sheet deglaciation. Rev. Geophys. 53, 1–48.

Patton, H., Hubbard, A., Andreassen, K., Winsborrow, M., Stroeven, A.P., 2016. The build-up, configuration, and dynamical sensitivity of the Eurasian ice-sheet complex to Late Weichselian climate and ocean forcing. Quat. Sci. Rev., 153, 97–121.

Patton, H., Hubbard, A., Andreassen, K., Auriac, A., Whitehouse, P. L., Stroeven, A. P., Shackleton, C., Winsborrow, M., Heyman, J., Hall., A. M., 2017. Deglaciation of the Eurasian ice sheet complex. Quat. Sci. Rev. 169, 148-172.

Perol, T., Rice, J. R., Platt, J. D., Suckale, J. 2015. Subglacial hydrology and ice stream margin locations. J. Geophys. Res. 120, 1352-1368.

Pfirman, S.L., Bauch, D., Gammelsrød, T., 2013. The northern Barents Sea: water mass distribution and modification. In The Polar Oceans and Their Role in Shaping the Global Environment. American Geophysical Union; 77–94.

Polyak, L., Lehman, S.J., Gataullin, V., Timothy Jull, A.J., 1995. Two-step deglaciation of the southeastern Barents Sea. Geology, 23(6), 567–571.

Piasecka, E.D., Winsborrow, M., Andreassen, K., Stokes, C.R., 2016. Reconstructing the retreat dynamics of the Bjørnøyrenna Ice Stream based on new 3D seismic data from the central Barents Sea. Quat. Sci. Rev. 151, 212-227.

Piotrowski, J.A., Larsen, N.K., Menzies, J., Wysota, W., 2006. Formation of subglacial till under transient bed conditions: deposition, deformation, and basal decoupling under a Weichselian ice sheet lobe, central Poland. Sedimentology, 53, 83–106.

Powell, R.D., Alley, R.B., 1997. Grounding-line systems: processes, glaciological inferences and the stratigraphic record. Geology and Seismic Stratigraphy of the Antarctic Margin, Part 2. Antarct. Res. Ser. 71, 169-187.

Powell, R.D., Domack, E.W., 1995. Modern glaciomarine environments. In: Menzies, J. (Ed.), Glacial Environments: Volume 1. Modern Glacial Environments: Processes, Dynamics and Sediments. Butterworth-Heinmann, Oxford, pp. 445–486.

Powell, R. D., Molnia, B. F., 1989. Glacimarine sedimentary proc- esses, facies and morphology of the south-southeast Alaska shelf and fjords. Marine Geology 85, 359–390

Reimer, P. J., Bard, E., Bayliss, A., Beck, J. W., Blackwell, P. G., Bronk Ramsey, C., Buck, C. E., Cheng, H., Edwards, R. L., Friedrich, M., Grootes, P. M., Guilderson, T. P., Haflidason, H., Hajdas, I., HattAŠ, C., Heaton, T. J., Hogg, A. G., Hughen, K. A., Kaiser, K. F., Kromer, B., Manning, S. W., Niu, M., Reimer, R. W., Richards, D. A., Scott, E. M., Southon, J. R., Turney, C. S. M., van der Plicht, J. 2013. IntCal13 and MARINE13 radiocarbon age calibration curves 0–50,000 years cal BP, Radio- carbon, 55, 1869–1887.

Rise, L., Knies, J., Baeten, N., Olsen, H. A., Bellec, V. K., Klug, M., 2016. Sedimentkjerner fra Barentshavet Øst tatt på MAREANO-tokt med G.O. Sars i 2014. NGU Rapport nr.: 2016.021. Norges Geologiske Undersøkelse. ISSN: 2387-3515

Robin, G. D., Swithinbank, C. W. M., Smith, B. M. E., 1970. Radio Echo Exploration of the Antarctic Ice Sheet, vol. 86, pp. 97–115, IASH publication, Hanover, N. H.

Röthlisberger, H., 1972. Water pressure in intra- and subglacial channels. Journal of Glaciology 11, 177–203.

Rüther, D.C., Mattingsdal, R., Andreassen, K., Forwick, M., Husum, K., 2011. Seismic architecture and sedimentology of a major grounding zone system deposited by the Bjørnøyrenna Ice Stream during Late Weichselian deglaciation. Quat. Sci. Rev., 30, 2776–2792.

Salvigsen, O., 1981. Radiocarbon dated raised beaches in Kong Karls Land, Svalbard, and their consequences for the glacial history of the Barents Sea area. Geografiska Annaler, 63, 283-291.

Sergienko, O. V., Hindmarsh, R. C. A., 2013. Regular patterns in frictional resistance of ice-stream beds seen by surface data inversion. Science 342, 1086-1089.

Shackleton, C., Patton, H., Hubbard, A., Winsborrow, M., Kingslake, J., Esteves, M., Andreassen, K., Greenwood, S. L., 2018. Subglacial water storage and drainage beneath the Fennoscandian and Barents Sea ice sheets. Quat. Sci. Rev. *In press*.

Siegert, M. J., 2000. Antarctic subglacial lakes. Earth-Science Reviews 50, 29 – 50.

Siegert, M. J., Carter, S., Tabacco, I., Popov, S., Blankenship, D.D., 2005. A revised inventory of Antarctic subglacial lakes, Antarct. Sci., 17(3), 453–460.

Siegert, M. J., Ross, N., Corr, H., Smith, B., Jordan, T., Bingham, R. G., Ferraccioli, F., Rippin, D. M., Le Brocq, A., 2014. Boundary conditions of an active West Antarctic subglacial lake: implications for storage of water beneath the ice sheet. The Cryosphere 8, 15–24.

Sigmond, E.M.O., 1992. Berggrunnskart, Norge med havområder. Målestokk 1:3 millioner. In Norges geologiske undersøkelse.

Simkins, L.M., Anderson, J.B., Greenwood, S.L., Gonnermann, H.M., Prothro, L.O., Halberstadt, A.R.W., Stearns, L.A., Pollard, D., DeConto, R.M., 2017. Anatomy of a meltwater drainage system beneath the ancestral East Antarctic ice sheet. Nat. Geosci. http://dx.doi.org/10.1038/NGEO3012.

Smith, B. E., Fricker, H. A., Joughin, I. R., Tulaczyk, S., 2009. An inventory of active subglacial lakes in Antarctica detected by ICESat (2003-2008). Journal of Glaciology 55 (192), 573 – 595.

Stearns, L.A., Smith, B.E. Hamilton, G.S., 2008. Increased flow speed on a large East Antarctic outlet glacier caused by subglacial floods. Nature Geoscience (1), 827–831.

Stuiver, M., Reimer, P.J., Reimer, R.W., 2017, CALIB 7.1 [WWW program] at http://calib.org, accessed 2017-06-15

Svendsen, J.I., Alexanderson, H., Astakhov, V.I., Demidov, I., Dowdeswell, J.A., Funder, S., Gataullin, V., Henriksen, M., Hjort, C., Houmark-Nielsen, M., Hubberten, H.W., Ingolfson, O., Jakobsson, M., Kjær, K.H., Larsen, E., Lokrantz, H., Lunkka, J.P., Lyså, A., Mangerud, J., Matiouchkov, A., Murray, A.S., Möller, P., Niessen, F., Nikolskaya, O., Polyak, L., Saarnisto, M., Siegert, C., Siegert, M.J., Spielhagen, R., Stein, R., 2004. Late Quaternary ice sheet history of northern Eurasia. Quat. Sci. Rev. 23, 1229–1271.

Tulaczyk, S., Kamb, W.B., Engelhardt, H.F. 2000. Basal mechanics of Ice Stream B, West Antarctica 1. Till mechanics, J. Geophys. Res., 105 (B1), 463-481.

Vaughan, D. G., Comiso, J.C., Allison, I., Carrasco, J., Kaser, G., Kwok, R., Mote, P., Murray, T., Paul, F., Ren, J., Rignot, E., Solomina, O., Steffen, K., Zhang, T., 2013. Observations: Cryosphere. In Climate Change 2013: The Physical Science Basis. Contribution of Working Group I to the Fifth Assessment Report of the Intergovernmental Panel on Climate Change [Stocker, T. F., Qin, D., Plattner, G.-K., Tignor, M., Allen, S.K., Boschung, J., Nauels, A., Xia, Y., Bex, V., and Midgley, P. M. (eds)]. Cambridge University Press, Cambridge, United Kingdom and New York, NY, USA.

Vorren,T.O., Hald,M., Lebesbye,E., 1988. Late Cenozoic environments in the Barents Sea. Paleoceanography, 3, 601–612.

Vorren, T.O., Lebesbye, E., Andreassen, K., Larsen, K.B., 1989. Glacigenic sediments on a passive continental margin as exemplified by the Barents Sea. Marine Geology, 85, 251–272.

Vorren, T.O., Laberg, J.S., 1997. Trough mouth fans – palaeoclimate and ice-sheet monitors. Quat. Sci. Rev., 16, 865–881.

Wadham, J.L., Bottrell, S., Tranter, M., Raiswell, R., 2004. Stable isotope evidence for microbial sulphate reduction at the bed of a polythermal high Arctic glacier. Earth and Planetary Science Letters 219, 341-355.

Weber, M. E., Niessen, F., Kuhn, G., Wiedicke, M., 1997. Calibration and application of marine sedimentary physical properties using a multi-sensor core logger, Mar. Geol. 136, 151–172.

Wingham, D. J., Siegert, M. J., Shepherd, A., Muir, A. S., 2006. Rapid discharge connects Antarctic subglacial lakes. Nature 440, 1033 – 1036.

Winsborrow, M.C.M., Andreassen, K., Corner, G.D., Laberg, J.S., 2010a. Deglaciation of a marine-based ice sheet: Late Weichselian palaeo-ice dynamics and retreat in the southern Barents Sea reconstructed from onshore and offshore glacial geomorphology. Quaternary Science Reviews, 29, 424-442.

Winsborrow, M. C. M., Clark, C. D., Stokes, C. R. 2010b. What controls the location of ice streams? Earth Sci. Rev. 103, 45–59.

Winsborrow, M.C.M., Stokes, C.R., Andreassen, K., 2012. Ice-stream flow switching during deglaciation of the southwestern Barents Sea. Geological Society of America Bulletin, 124, 275-290.

Wright, A., Siegert, M. J., 2012. A fourth inventory of Antarctic subglacial lakes. Antarctic Science 24 (6), 659-664.

Zwally, H. J., Abdalati, W., Herring, T., Larson, K., Saba, J., Steffen, K., 2002. Surface Melt-Induced Acceleration of Greenland Ice-Sheet Flow. Science 297, 218 – 222.